International Journal of Hydrogen Energy 111 (2025) 142–158

Contents lists available at ScienceDirect

International Journal of Hydrogen Energy

journal homepage: www.elsevier.com/locate/he

Optimal configuration of hydrogen- and battery-based electric bus transit systems

Ahmed Foda [a,b,c,*], Moataz Mohamed [a], Hany E.Z. Farag [d], Patrick Jochem [e], Elkafi Hassini [b]

[a] Department of Civil Engineering, McMaster University, 1280 Main Street West, Hamilton, L8S 4L8, Canada
[b] DeGroote School of Business, McMaster University, 1280 Main Street West, Hamilton, L8S 4L8, Canada
[c] Department of Mathematics & Engineering Physics, Mansoura University, Mansoura, 35516, Egypt
[d] Electrical Engineering and Computer Science Department, York University, Toronto, ON, M3J 1P3, Canada
[e] Institute of Networked Energy Systems, German Aerospace Center (DLR), Curiestr. 4, 70563, Stuttgart, Baden-Württemberg, Germany

ARTICLE INFO

Handling Editor: Ramazan Solmaz

Keywords:
Battery electric buses (BEBs)
Hydrogen fuel cell buses (HFCBs)
Transit electrification
Optimal system configuration

ABSTRACT

Electric bus transit is crucial in reducing greenhouse gas (GHG) emissions, decreasing fossil fuel reliance, and combating climate change. However, the transition to electric-powered buses demands a comprehensive plan for optimal resource allocation, technology choice, infrastructure deployment, and component sizing. This study develops system configuration optimization models for battery electric buses (BEBs) and hydrogen fuel cell buses (HFCBs), minimizing all related costs (i.e., capital and operational costs). These models optimize component sizing of the charging/refueling stations, fleet configuration, and energy/fuel management system in three operational schemes: BEBs opportunity charging, BEBs overnight charging, and electrolysis-powered HFCBs overnight refueling. The results indicate that the BEB opportunity system is the most economically viable choice. Meanwhile, HFCB requires a higher cost (134.5%) and produces more emissions (215.7%) than the BEB overnight charging system. A sensitivity analysis indicates that a significant reduction in the HFCB unit and electricity costs is required to compete economically with BEB systems.

1. Introduction

Rising concerns over climate change and dwindling energy resources are pushing industry and research toward a stronger focus on environmental sustainability and energy efficiency. Decarbonizing the transportation sector and overcoming fossil fuel dependence are key challenges for achieving sustainable cities. In 2022, Canada's transportation sector contributed significantly to greenhouse gas (GHG) emissions, emitting approximately 22% of the total national emissions [1], and similar rates are observed globally in terms of GHG emissions and energy demand shares [2].

In this context, transitioning to electric buses is a promising solution to reduce GHG emissions as it enhances energy efficiency and allows for higher fuel flexibility [3,4]. Electric buses, such as battery electric buses (BEBs) and hydrogen fuel cell buses (HFCBs), can significantly eliminate GHG emissions, provide quiet operation, and enhance urban area air quality [5]. Although BEBs are rapidly gaining market share (91.1% of the global electric bus market in 2023) [6], they face some challenges centered around the limited driving range and extended charging times. En-route charging is often recommended through high-power fast chargers to overcome the need for larger battery capacities [7]. Despite that, utilizing high-power chargers during operation negatively impacts the battery lifetime and electricity grid and could lead to higher electricity/operational costs [8]. In comparison, HFCBs offer an extended operational range comparable with fossil fuel buses without the need for refueling during operation, addressing key limitations associated with BEBs [9]. However, concerns regarding the cost of hydrogen production and HFCB units remain, creating an obstacle to its broad use [10,11].

In this respect, a comprehensive electrification plan for BEBs and/or HFCBs requires sophisticated optimization models to assess the capital (CAPEX) and operational (OPEX) costs for each technology. Moreover, choosing between these two zero-emission transit systems requires careful consideration of factors, including economic, environmental, and operational aspects, as well as the specific needs of the transit

* Corresponding author. Department of Civil Engineering, McMaster University, 1280 Main Street West, Hamilton, L8S 4L8, Canada.
E-mail addresses: fodaa@mcmaster.ca (A. Foda), mmohame@mcmaster.ca (M. Mohamed), hefarag@yorku.ca (H.E.Z. Farag), Patrick.Jochem@dlr.de (P. Jochem), hassini@mcmaster.ca (E. Hassini).

https://doi.org/10.1016/j.ijhydene.2025.02.251
Received 9 December 2024; Received in revised form 14 February 2025; Accepted 15 February 2025
Available online 25 February 2025

operation.

The literature lacks comparative analyses of the optimal system configuration for BEBs and HFCBs and energy/fuel management [5], underscoring a significant research gap. Therefore, this work provides a comprehensive applied methodology to address the following questions:

1) What is the optimal system configuration for an electrified transit network (charging/refueling stations and fleet) for BEB or HFCB systems? Moreover, what charging/refueling schedules are necessary to meet fleet energy/fuel demand?
2) What is the power demand from the electricity grid, and what is the impact of charging/refueling stations on the grid? Additionally, how significant are the well-to-tank (WTT) GHG emissions?
3) Which electrification option is most suitable for the transit network, considering budget constraints (economic), emission reduction targets (environmental), compatibility with the electricity network, and operational flexibility with the service timetable?

To address these questions, two generic zero-emission transit system configuration models for infrastructure and energy/fuel management are proposed while adhering to the operational timetable of the transit network. Consequently, a comparative evaluation of the two systems is conducted.

2. Literature review

The literature review is discussed in three sections, reflecting on recent work on system configuration research for BEB and HFCB independently, as well as the joint integration of both systems in one study.

2.1. Battery electric bus system configuration

BEB system configuration research is dominant in the transit electrification literature. For the BEB system, the research has widely covered multiple topics, including BEB fleet sizing and scheduling [12–14], fleet configuration [15,16], infrastructure allocation [17,18], component sizing of the charging system [7,19], charging scheduling [20,21], mitigating impact on the electricity grid [22,23] and battery degradation [13,24,25], system robustness and resilience [26–28], and integration between some of them. These studies offer tangible contributions to BEB system configuration. The literature also highlights the economic and environmental benefits, supporting broader adoption and improved effectiveness.

One stream of research focuses on optimizing charging stations and fleet configurations to reduce the total cost of ownership (TCO). This includes the sizing of the transformer and converter, charger unit-rated power, the number of outlets, and fleet battery capacity. However, various models were proposed in terms of which components are quantified as decision variables and which are treated as predefined variables. For example, in Refs. [29–31], the number of outlets is optimized while charger power and fleet battery capacity/range are set to predefined values. Moreover, energy storage systems (ESSs) are introduced in Refs. [32–34] to help reduce the system's TCO. However, recent research highlights that optimizing all charging station components and fleet configuration enables a balanced approach, ultimately reducing the TCO [7,19].

Another stream optimizes the fleet charging schedule [35,36]. The optimal charging schedule considers the spatiotemporal and operational parameters of the charging events to minimize the electricity time-of-use (ToU) cost [37], peak power demand [38], WTT GHG emissions [39], and the impact on the electricity grid [7]. Recently, a few studies have proposed integrated models that jointly optimize the BEB system infrastructure and charging schedule to minimize the TCO [16,40].

However, integrating BEB system optimization with other technologies, such as HFCB, was rarely discussed in the literature.

2.2. Hydrogen fuel cell bus system configuration

The research in hydrogen systems has mainly focused on the allocation of hydrogen refueling stations (HRSs) and optimizing their components and operations.

The optimal allocation of HRSs, considering transit and non-transit systems, has been investigated using node-based [41,42] and link-based allocation models [43–45]. For instance, in Ref. [42], a node-based multi-period p-median model is developed to estimate the number and the location of HRSs that minimize the long-term planning investment, considering the human development index and traffic flow for fuel demand estimation. In Ref. [43], a link-based optimization model is proposed for planning a sustainable refueling network for multiple types of fuels, considering total cost, environmental pollution, and social welfare as objective functions. A multi-objective and multi-period long-term planning model for the HRS location problem has been developed in Ref. [46] to optimize total costs, risk, and population coverage. In Ref. [47], the optimal locations of HRSs are estimated using multi-objective analysis, considering economic, environmental, and safety aspects, and based on the locations of existing natural gas stations and the hydrogen demand of the targeted HFCB fleet size.

Another line of research focused on optimizing the component sizing and operation of HRSs. This includes electrolyzer, compressors, hydrogen storage, renewable energy sources, and stationary ESSs [48–50]. For example, the work in Ref. [50] minimizes the total cost of hydrogen (CoH) by optimizing the electrolyzer sizing, while in Ref. [51], the CoH is reduced by enhancing the electrolyzer's conversion efficiency.

The work in Ref. [52] minimizes the investment cost by optimizing the integration of RESs (photovoltaic) and diesel generators in a hybrid refueling station for hydrogen and electric vehicles while considering uncertainty. In Ref. [53], a wind- and solar-powered HRS design for a hydrogen- and diesel-powered bus fleet is developed. This robust design optimization model aims to minimize the levelized cost of driving and the carbon intensity, considering the uncertainties of technical, cost, and environmental parameters. Furthermore, The work in Ref. [54] minimizes the levelized cost of hydrogen using techno-economic modelling for a nationwide hydrogen fuel supply chain, including hydrogen production, transportation, and dispensing systems, to meet HFCB demand in specific cities in Ireland. Wind farms are selected as HRS locations, and the electrolyzer, photovoltaic array, and stationary ESSs are optimized.

However, there is still a lack of a transit-based hydrogen refueling model that integrally optimizes the HRS components and operation, refueling schedules, and fleet configuration while considering the transit network operational schedule.

2.3. Comparative studies between battery electric and hydrogen fuel cell systems

Indeed, several research studies have provided a lifecycle assessment of zero-emission buses, including BEBs and HFCBs [55–58]. However, the literature search on comparative assessment between the optimal systems (BEB and HFCB) configurations returned a few recent studies [5, 59–61]. A summary of these relevant studies is presented in Table 1.

In [5], a data-driven micro-simulation framework is proposed to compare BEB and HFCB transit systems. The BEB/HFCB operation is simulated, and then the results from the simulations are imported into the charging/refueling station location optimization models. For the BEB system, a bi-objective model is formulated to minimize the system costs and maximize the service level. This model provides the optimal locations of the charging stations, the configuration of each location (i.e., number and power of chargers), and fleet scheduling. For the HFCB system, an allocation optimization model is developed to minimize system costs. However, the configuration of the HRS is not considered in

Table 1
Summary of most relevant studies.

Study	HRS configuration	HFCBs configuration	charging station configuration	BEBs configuration	Energy/fuel management
[5]	Not optimized	Not optimized	Number of chargers Power of chargers	Not optimized	Simulated
[59]	Average number of dispensers Electrolyzer power Hydrogen storage tank Compressor specifications	Bus tank size	Not optimized	Not optimized	Refueling schedule
[60]	PV system Wind system Electrolyzer power Compressor power Hydrogen storage tank	Not optimized	PV system Wind system ESS specifications	Not optimized	Refueling schedule
[61]	Number of PV panels ESS capacity Hydrogen storage tank	Not optimized	Number of PV panels ESS capacity	Not optimized	Refueling and charging schedules
This study	Transformer power Converter power Electrolyzer power Compressor power Hydrogen storage tank Number of dispensers	Bus tank size	Transformer power Converter power ESS capacity Charger power Number of outlets	Battery capacity	Refueling and charging schedules

this study. Moreover, in both models, the fleet configuration is not optimized.

In [59], an algorithm for the HRS design is proposed to minimize the levelized cost of hydrogen (LCOH), considering the electricity and investment costs associated with hydrogen demand given by different HFCB fleet sizes and electrolyzer-rated powers. A techno-economic model is developed as an evolutionary algorithm with step-by-step instructions in MATLAB. At the start of the algorithm, the bus tank capacity is defined, refueling time and the average number of dispensers are quantified according to the fleet size, tank size is assumed to accommodate three days of production, and the compressor parameters are set. Then, under different electrolyzer and fleet sizes, an LCOH matrix is generated by associating the minimum average electricity price with the number of operating hours of the electrolyzer and the compressor. However, the model does not consider the fleet's operational timetable or simultaneously optimize the HRS's components and operations. Although a cost comparison between the HFCB fleet refueling and BEB fleet recharging was performed in this study, the analysis did not include the fleet costs, nor did it quantify the optimal BEB system configuration.

A comparative analysis between the BEB and HFCB systems is performed in Ref. [60], with charging/refueling infrastructures in a remote off-grid context. The assessment involves the sizing of renewable energy sources (i.e., photovoltaic and wind) and the HRS or BEB charging station. The proposed techno-economic simulation and optimization is conducted using a toolbox called PyPSA. For BEBs charging, the proposed simulation optimizes the stationary ESSs. However, the charger-rated power is assumed to be a constant value. Moreover, a predefined load profile from the BEB system is assumed, limiting the generated results. Meanwhile, for HFCB refueling stations, the electrolyzer, compressor, and hydrogen storage sizes are optimized. However, the fleet configuration is not optimized for both systems, and the associated costs are not considered in the comparison.

An energy management approach for stand-alone and grid-connected charging/refueling station that serves BEBs and HFCBs has been developed in Ref. [61]. This energy management approach is based on a charging/refueling schedule designed by an imperative priority system, considering the bus state of charge, parking time, and next trip energy consumption. The proposed model optimizes the stationary ESS (in the stand-alone case), hydrogen storage tank, and the number of photovoltaic panels. However, the developed model does not consider the optimal fleet configuration and other charging/refueling station components (e.g., charger, electrolyzer, and compressor).

This literature review highlights a research gap for a comprehensive comparative analysis of BEB and HFCB transit system configurations. Precisely, optimizing the system configuration while jointly considering the following aspects has not been developed yet. There are no current models that consider a) integrating transit network spatiotemporal demand (operation timetable), b) optimizing all the daily operational schedules of the charging/refueling station, c) considering all charging/refueling station components as decision variables, and d) including the fleet configuration (battery capacity or hydrogen tank sizing) and costs.

2.4. Detailed contribution

This research develops two generic system configuration optimization models for BEBs and HFCBs that optimize the system's infrastructure, planning, and operation. The proposed models aim to minimize the total annual system costs, including CAPEX and OPEX, while maintaining the operational timetable of the transit network. Compared to the existing literature, this study contributes to the following:

1) A detailed BEB system optimization for charging station and fleet configurations, including the rated power of the transformer, converter, and charger unit, the number of outlets, ESS capacity, if it exists, and battery capacities. Moreover, the model optimizes the energy management system, including a bidirectional charging schedule for the ESS and the charging schedule of the BEBs (when, where, how long, and how much).
2) A detailed HFCB system optimization for on-site hydrogen production/refueling station and fleet configurations, including the rated power of the transformer, converter, electrolyzer, and compressor, hydrogen storage tank size, number of dispensers, and the HFCB tank size. Moreover, the model optimizes the energy/fuel management system, including the power dispatch schedules to the electrolyzer and compressor, hydrogen production and storage, and HFCB fleet refueling.
3) A sensitivity analysis to compare the performance of the two systems. The analysis assesses how variations in HFCB unit and electricity costs impact the total annual system costs, identifying cost ranges that make the HFCB system financially competitive with the BEB system.

Following the introduction and background, the rest of the study is structured as follows. Section 2 presents the methodology, including the detailed formulation of the proposed optimization models for the two zero-emission bus systems. Section 3 discusses the case study and the results of applying the proposed models. Section 4 provides a

competitiveness assessment between the two systems. Finally, Section 5 concludes with key findings and highlights of this research.

3. Methodology

A zero-emission transit system includes three main components: a transit network consisting of routes, stops, a timetable, charging/refueling stations, and a fleet of zero-emission buses. A hub-and-spoke transit network, considered in this work, could be defined by a set of routes served by a fleet of buses ($b \in B$) that fulfill predetermined trips ($i \in I_b, \forall b \in B$). Overnight, buses are housed at the depot, while during operation, they recover between scheduled trips at the terminal or central station. Therefore, the first and last trips are deadhead trips between the depot and the terminal (central station).

The configuration of the charging/refueling stations depends on the type of the zero-emission fleet. This work proposes two models: one for configuring a BEB fleet with the necessary charging station and another for configuring an HFCB fleet with the required refueling station. The two proposed models aim to minimize CAPEX, OPEX, impacts on the electricity grid, and the social cost of GHG emissions while satisfying the fleet spatiotemporal energy/fuel demand.

Notably, our study considers three charging/refueling schemes (Fig. 1): BEB opportunity charging, BEB overnight charging, and HFCB overnight refueling.

- For BEB opportunity charging, two charging stations are deployed—one at the depot for overnight charging and another at the terminal for charging events during recovery times between trips, if needed.
- For BEB overnight charging, a single charging station at the depot is utilized.
- For HFCB overnight refueling, one refueling station with a hydrogen production plant at the depot is deployed.

The proposed models are based on three assumptions following zero-emission bus transit practice. These include:

1) The operation must adhere to the transit timetable with the same number of buses [7,17,62].
2) The transit network follows a hub-and-spoke structure with a single terminal and depot [21,37].
3) The fleet is fully charged/fueled before leaving the depot [21,39].

3.1. Modelling battery electric bus system

3.1.1. Problem description

The proposed model integrally quantifies the optimal configuration of the charging system, the BEB fleet, and the optimal charging schedule. The charging system consists of two stations located at the depot ($s = 1$, $s \in S$) and the terminal ($s = 2$, $s \in S$), where $S = \{1, 2\}$ is the set of charging stations. The depot charging station is used for overnight charging, while the terminal charging station is utilized during recovery time between trips.

The optimal components of the charging station $s \in S$ include the transformer-rated power ($P_s^{rated,tr}$), the converter-rated power ($P_s^{rated,conv}$), the energy storage system-rated capacity (E_s^{ESS}), the charging station rated power ($P_s^{rated,st}$), and the number of outlets (N_s^{pil}). In addition, the model provides the optimal battery size (E_b^{batt}) of each BEB ($b \in B$). A holistic system structure is depicted in Fig. 2.

The proposed BEB model provides the optimal management of the power dispatch in the charging system, including the bidirectional charging schedule of the ESS (if deployed) and the charging schedule of the BEBs. The fleet charging schedule follows the partial and continuous charging concepts [7]. Therefore, the charging duration and power are considered decision variables in the proposed model. Toward this end, a generic BEB system configuration model is formulated as a mixed integer linear programming model. The notations of the BEB model are shown in Table 2.

3.1.2. Objective function

The BEB system configuration model aims to minimize the total annual system costs (F^{Total}) in (1), consisting of two components: CAPEX and OPEX, presented in (2) and (3), respectively. Where r is the discount rate, y is the components' lifespan, and N^{days} is the number of operational days.

$$F^{total} = \frac{r(1+r)^y}{(1+r)^y - 1} CAPEX + N^{days} OPEX \tag{1}$$

CAPEX comprises six terms as described in (2). The first term represents the fixed construction cost of the charging stations (α^{con}) followed by the transformer cost (α^{tr}), which is a function of the transformer-rated power ($P_s^{rated,tr}$). The third term presents the converter cost (α^{conv}), while the fourth term introduces the charging unit costs, including the costs related to the charger-rated power (α^{BC}) and the number of outlets (α^{pil}). Lastly, the fifth term presents the ESS cost, if it exists, and the last term describes the BEB fleet costs considering the bus cost without battery (α^{BEB}) and the battery cost (α^{batt}) according to its capacity.

$$\begin{aligned} CAPEX = & \sum_{s\in S} \alpha^{con} + \sum_{s\in S} \alpha^{tr} P_s^{rated,tr} + \sum_{s\in S} \alpha^{conv} P_s^{rated,conv} \\ & + \sum_{s\in S} \left[\alpha^{BC} P_s^{rated,st} + \alpha^{pil} N_s^{pil}\right] + \sum_{s\in S} \alpha^{ESS} E_s^{ESS} + \sum_{b\in B} \left(\alpha^{batt} E_b^{batt} + \alpha^{BEB}\right) \end{aligned} \tag{2}$$

In the proposed model, OPEX includes the electricity cost and the social cost of GHG emissions. The first part of the electricity costs comprises the fixed and variable rates of electricity related to the charging energy. For example, in Ontario, Canada, this parameter, α_t^{elect}, includes several factors, such as the hourly energy price and global adjustment rate. The second cost parameter presents the daily peak power demand charges. The social cost of GHG emissions is described in the last part of the OPEX as a function of the charged energy and the ToU.

$$OPEX = \sum_{s\in S} \sum_{t\in T} \left[\alpha_t^{elect} \Delta TP_{t,s}^{conv} + \alpha^{dem} P_s^{dem}\right] + \sum_{s\in S} \sum_{t\in T} \alpha_t^{em} \Delta TP_{t,s}^{conv} \tag{3}$$

The objective function of the proposed BEB model in (1) is optimized under a set of constraints presented in (4–30).

3.1.3. BEB system's constraints

For each BEB $b \in B$, the battery energy is constrained by (4-8), the charging power by (9-10), and the charging event by (11-13). The battery energy of each BEB b during operation is constrained within a predefined range relative to the bus's battery capacity, specifically between $\xi_{min}^{batt} E_b^{batt}$ and $\xi_{max}^{batt} E_b^{batt}$, as specified in constraints (4-5). However, in (6), the initial departure battery energy from the depot ($s = 1$) for the deadhead trip to the terminal ($i = 1$) equals the maximum battery energy level. For each BEB during operation, the battery energy is updated according to (7–8). In (7), the arrival energy of BEB $b \in B$ at station $s \in S$ after completing trip $i \in I_b$ ($E_{b,i,s}^{arr}$) equals the departure energy from station s' for the same trip ($E_{b,i,s'}^{dep}$) minus the energy consumed during the trip. The energy consumption is calculated as the product of the trip distance $l_{b,i}$ and the energy consumption rate, which includes both a fixed part and a variable part related to the battery size. In addition, the departure energy of bus b from station s for trip $i+1$ equals the summation of the energy upon arrival and the energy acquired through charging at the station, if available.

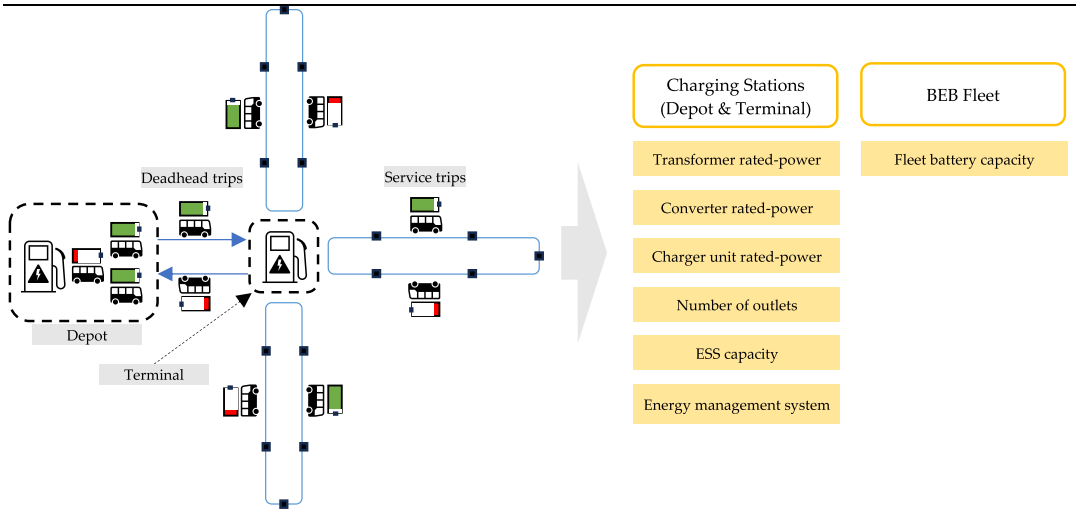

a) BEB opportunity charging transit system

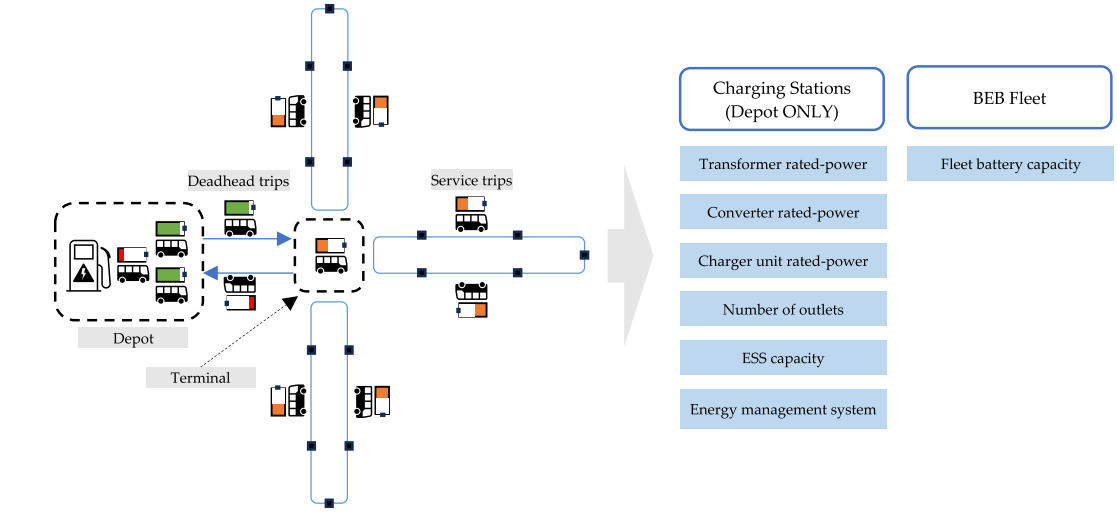

b) BEB overnight charging transit system

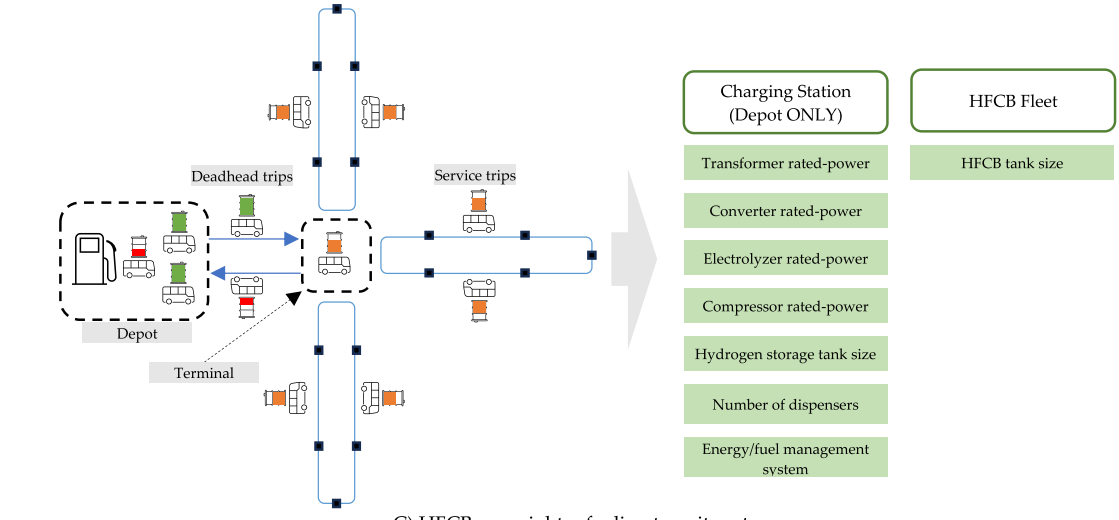

C) HFCB overnight refueling transit system

Fig. 1. Charging/Refueling systems.

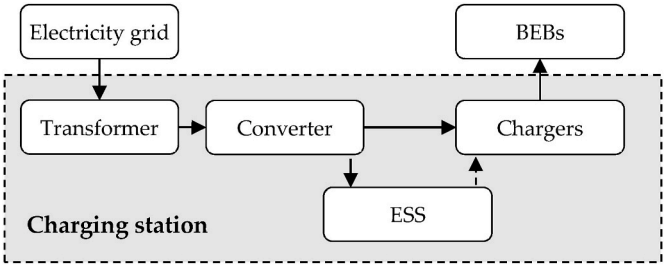

Fig. 2. BEB charging station design.

$$E^{arr}_{b,i,s} \geq \xi^{batt}_{min} E^{batt}_{b} \quad \forall b \in B, \forall i \in I_b, s \in S \tag{4}$$

$$E^{dep}_{b,i,s} \leq \xi^{batt}_{max} E^{batt}_{b} \quad \forall b \in B, \forall i \in I_b, s \in S \tag{5}$$

$$E^{dep}_{b,1,1} = \xi^{batt}_{max} E^{batt}_{b} \quad \forall b \in B \tag{6}$$

$$E^{arr}_{b,i,s} = E^{dep}_{b,i,s'} - l_{b,i}\left(e^{fix}_{b,i} + e^{batt} E^{batt}_{b}\right) \quad \forall b \in B, \forall i \in I_b, s, s' \in S \tag{7}$$

$$E^{dep}_{b,i+1,s} = E^{arr}_{b,i,s} + \sum_{t \in R_{b,i,s}} \eta^{BC} \Delta T P^{ch}_{b,i,s,t} \quad \forall b \in B, \forall i \in I_b, s \in S \tag{8}$$

The charging power of bus b after trip i in location s during timeslot t ($P^{ch}_{b,i,s,t}$) is constrained by (9-10). According to (9), $P^{ch}_{b,i,s,t}$ is restricted to be lower than an upper factor multiplied by the BEB battery capacity (C-rate). Moreover, $P^{ch}_{b,i,s,t}$ is controlled to be in a predefined range $\left[P^{ch,min}, P^{max,pil}\right]$, if the bus is charging, as mentioned in (10). The continuity of the charging event, if the bus charges, in each recovery time ($R_{b,i,s}$) is imposed using the auxiliary variables $\theta^{ch}_{b,i,s,t}$ and $\rho^{ch}_{b,i,s,t}$ in the Constraints (11-13) [7,21].

$$P^{ch}_{b,i,s,t} \leq \mu^{ch} E^{batt}_{b} \quad \forall b \in B, \forall i \in I_b, \forall t \in R_{b,i,s}, s \in S \tag{9}$$

$$P^{ch,min} x_{b,i,s,t} \leq P^{ch}_{b,i,s,t} \leq P^{max,pil} x_{b,i,s,t} \quad \forall b \in B, \forall i \in I_b, \forall t \in R_{b,i,s}, s \in S \tag{10}$$

$$\theta^{ch}_{b,i,s,t} \geq x_{b,i,s,t} - x_{b,i,s,t+1} \quad \forall b \in B, \forall i \in I_b, \forall t \in R_{b,i,s}, s \in S \tag{11}$$

$$\rho^{ch}_{b,i,s,t} \geq x_{b,i,s,t} - x_{b,i,s,t-1} \quad \forall b \in B, \forall i \in I_b, \forall t \in R_{b,i,s}, s \in S \tag{12}$$

$$\sum_{t \in R_{b,i,s}} \theta^{ch}_{b,i,s,t} = \sum_{t \in R_{b,i,s}} \rho^{ch}_{b,i,s,t} \leq 1 \quad \forall b \in B, \forall i \in I_b, s \in S \tag{13}$$

In (14), the active power balance is enforced. The input power, comprising the grid power ($P^{grid}_{t,s}$) and the discharging power from the ESS ($P^{ESS,dis}_{t,s}$), should be equal to the output power, which includes the charging powers of both the ESS ($P^{ESS,ch}_{t,s}$) and the charging station ($P^{st,ch}_{t,s}$), and losses of the transformer ($(1-\xi^{tr})P^{grid}_{t,s}$) and the converter ($(1-\xi^{conv})\,P^{conv}_{t,s}$). It is noteworthy that only the ESS charging ($P^{ESS,ch}_{t,s}$) or discharging ($P^{ESS,dis}_{t,s}$) event can take place at any timeslot t, as governed by (24-27).

$$P^{grid}_{t,s} = P^{st,ch}_{t,s} + P^{ESS,ch}_{t,s} - P^{ESS,dis}_{t,s} - (1-\xi^{tr})P^{grid}_{t,s} - (1-\xi^{conv})\,P^{conv}_{t,s} \quad \forall s \in S, \forall t \in T \tag{14}$$

The active power consumed from the grid at location s during every timeslot t ($P^{grid}_{t,s}$) is related to the transformer-rated power ($P^{rated,tr}_{s}$), as stated in (15). Similarly, in (16), the input power to the converter $\left(P^{conv}_{t,s}\right)$ is also related to the converter-rated power ($P^{rated,conv}_{s}$). Moreover, the relation between the consumed power from the grid ($P^{grid}_{t,s}$) and the input power to the converter ($P^{conv}_{t,s}$) is controlled in (17).

$$P^{grid}_{t,s} \leq P^{rated,tr}_{s} \quad \forall s \in S, \forall t \in T \tag{15}$$

$$P^{conv}_{t,s} \leq P^{rated,conv}_{s} \quad \forall s \in S, \forall t \in T \tag{16}$$

$$P^{conv}_{t,s} = \xi^{tr} P^{grid}_{t,s} \quad \forall s \in S, \forall t \in T \tag{17}$$

In (18), the number of BEBs charging during the timeslot t at location s should be less than or equal to the number of allocated charging outlets (N^{pil}_{s}). Moreover, the total charging power for all BEBs at the same location and timeslot should equal the charging power at the station ($P^{st,ch}_{t,s}$) and remain below the rated power of the charger unit ($P^{rated,st}_{s}$), as demonstrated in (19).

$$\sum_{b \in B} x_{b,i,s,t} \leq N^{pil}_{s} \quad \forall s \in S, i \in I_b, \forall t \in T \tag{18}$$

$$\sum_{b \in B} P^{BC}_{b,i,s,t} = P^{st,ch}_{t,s} \leq P^{rated,st}_{s} \quad \forall s \in S, i \in I_b, \forall t \in T \tag{19}$$

The ESS energy level is constrained by (20-22) if it exists in location s. In (20), the ESS energy level ($E^{ESS,l}_{t,s}$) is constrained to a predefined range related to its capacity (E^{ESS}_{s}). However, $E^{ESS,l}_{t,s}$ is restricted to equal the upper limit in the first timeslot ($t = 1$), with the ESS charging overnight to this limit in preparation for the next day (21). In each timeslot t and location s, the ESS energy level is updated according to (22). The ESS energy level at timeslot $t+1$ equals the summation of the ESS level and the charged energy at timeslot t minus the discharged energy, where $P^{ESS,dis}_{t,s}$ is the ESS discharging power, and $P^{ESS,ch}_{t,s}$ is the ESS charging power.

$$\xi^{ESS}_{min} E^{ESS}_{s} \leq E^{ESS,l}_{t,s} \leq \xi^{ESS}_{max} E^{ESS}_{s} \quad \forall s \in S, \forall t \in T \tag{20}$$

$$E^{ESS,l}_{1,s} = \xi^{ESS}_{max} E^{ESS}_{s} \; \forall s \in S \tag{21}$$

$$E^{ESS,l}_{t+1,s} = E^{ESS,l}_{t,s} - \Delta T \frac{P^{ESS,dis}_{t,s}}{\eta^{ESS,dis}} + \eta^{ESS,ch} \Delta T\, P^{ESS,ch}_{t,s} \quad \forall s \in S, \forall t \in T \tag{22}$$

Similar to the BEB charging power, the ESS charging and discharging powers are restricted by (23-24) and (25–26), respectively. Here, the ESS charging/discharging power should be less than an upper limit related to the ESS capacity (E^{ESS}_{s}) or a predefined cap ($P^{max,ESS}$). In (27), the ESS is allowed to either charge or discharge in each timeslot, where $y_{t,s}$ is a binary variable that indicates whether the ESS is charging while $z_{t,s}$ is a binary variable that indicates whether the ESS is discharging.

$$P^{ESS,ch}_{t,s} \leq \mu^{ESS,ch} E^{ESS}_{s} \quad \forall s \in S, \forall t \in T \tag{23}$$

$$P^{ESS,ch}_{t,s} \leq P^{max,ESS} y_{t,s} \quad \forall s \in S, \forall t \in T \tag{24}$$

$$P^{ESS,dis}_{t,s} \leq \mu^{ESS,dis} E^{ESS}_{s} \quad \forall s \in S, \forall t \in T \tag{25}$$

$$P^{ESS,dis}_{t,s} \leq P^{max,ESS} z_{t,s} \quad \forall s \in S, \forall t \in T \tag{26}$$

$$y_{t,s} + z_{t,s} \leq 1 \quad \forall s \in S, \forall t \in T \tag{27}$$

Let J denotes the set of intervals to calculate the daily peak power demand. In (28), the average power demand from the electricity grid in interval j and location s ($P^{avg}_{j,s}$) is estimated, where $\left|T_j\right|$ is the number of timeslots in interval $j \in J$. As such, the peak power demand is calculated using (29).

$$P^{avg}_{j,s} = \frac{\sum_{t \in T_j} P^{conv}_{t,s}}{\left|T_j\right|} \quad \forall s \in S, \forall j \in J \tag{28}$$

$$P^{dem}_{s} \geq P^{avg}_{j_s} \quad \forall s \in S, \forall j \in J \tag{29}$$

Table 2
BEB model notations.

Sets	Description
B	Set of Buses, indexed by b
T	Set of day timeslots, indexed by t
I_b	Set of trips of bus b, indexed by i
S	Set of charging stations, indexed by s
$R_{b,i,s}$	Set of recovery timeslots of bus b after trip i in station s
J	Set of daily demand measurement intervals, indexed by j
T_j	Set of timeslots in demand measurement interval j
A^{tr}	Set of potential transformer-rated power values
A^{conv}	Set of potential converter-rated power values
A^{st}	Set of potential charger-rated power values
A^{ESS}	Set of potential ESS capacity values
A^{batt}	Set of potential battery capacity values

Parameters	Description	Parameters	Description
r	Discount rate (%)	μ^{ch}, $\mu^{ESS,ch}$, $\mu^{ESS,dis}$	Upper factor of bus charging, ESS charging, and ESS discharging related to the bus battery and ESS capacities, respectively (#)
y	Lifespan in years (#)	$P^{max,pil}$	Maximum bus charger power (kW)
N^{days}	Number of working days per year (#)	ξ^{tr}	Transformer efficiency (%)
α^{con}	Construction cost ($)	ξ^{conv}	Converter efficiency (%)
α^{tr}	Transformer cost ($/kW)	ξ^{ESS}_{min}, ξ^{ESS}_{max} ξ^{batt}_{min}, ξ^{batt}_{max}	Limits (%)
α^{conv}	Converter cost ($/kW)	$l_{b,i}$	Length of trip i of bus b (km)
α^{BC}	BEB charger cost ($/kW)	η^{ch}	BEB charger efficiency (%)
α^{pil}	Pile cost ($/unit)	$\eta^{ESS,dis}$	ESS discharging efficiency (%)
α^{ESS}	ESS cost ($/kWh)	$\eta^{ESS,ch}$	ESS charging efficiency (%)
α^{batt}	Battery cost ($/kWh)	$P^{max,ESS}$	Maximum charging/discharging power for ESS (kW)
α^{BEB}	BEB cost (without the battery) ($/unit)	$P^{ch,min}$	Minimum charging power (kW)
α^{elect}_t	Electricity cost during timeslot t ($/kWh)	α^{em}_t	Grid WTT social cost of GHG emissions during timeslot t ($/kWh)
ΔT	Timeslot duration (hr)	e^{batt}	Energy consumption rate due to the battery size (#)
α^{dem}	Demand charge rate ($/kW)	$e^{fix}_{b,i}$	Energy consumption rate of trip i of bus b (kWh/km)

Decision variables	Description
$P^{rated,tr}_s$	Transformer-rated power in station s (kW), $P^{rated,tr}_s \in A^{tr}$
$P^{rated,conv}_s$	Converter-rated power in station s (kW), $P^{rated,conv}_s \in A^{conv}$
$P^{rated,st}_s$	BEB charger unit rated power in station s (kW), $P^{rated,st}_s \in A^{st}$
E^{ESS}_s	ESS capacity in station s (kWh), $E^{ESS}_s \in A^{ESS}$
E^{batt}_b	BEB b battery capacity (kWh), $E^{batt}_b \in A^{batt}$
N^{pil}_s	Number of outlets in station s (#), $N^{pil}_s \in \mathbb{Z}_{>0}$
$P^{grid}_{t,s}$	Power demand from the grid at timeslot t in station s (kW), $P^{grid}_{t,s} \geq 0$
P^{dem}_s	Peak power demand t in station s (kW), $P^{dem}_s \geq 0$
$P^{ESS,ch}_{t,s}$	ESS charging power at timeslot t in station s (kW), $P^{ESS,ch}_{t,s} \geq 0$
$P^{ESS,dis}_{t,s}$	ESS discharging power at timeslot t in station s (kW), $P^{ESS,dis}_{t,s} \geq 0$
$P^{st,ch}_{t,s}$	Total BEBs charging power at timeslot t in station s (kW), $P^{st,ch}_{t,s} \geq 0$
$P^{conv}_{t,s}$	Converter input power at timeslot t in station s (kW), $P^{conv}_{t,s} \geq 0$
$P^{ch}_{b,i,s,t}$	Charging power for bus b after trip i in station s during timeslot t (kW), $P^{ch}_{b,i,s,t} \geq 0$
$x_{b,i,s,t}$	A Binary decision variable indicates whether bus b is charging after trip i in station s during timeslot t or not, $x_{b,i,s,t} \in \{0,1\}$
$y_{t,s}$	Binary decision variable indicates whether the ESS in station s is charging or not, $y_{t,s} \in \{0,1\}$
$z_{t,s}$	Binary decision variable indicates whether the ESS in station s is discharging or not, $z_{t,s} \in \{0,1\}$
$\theta^{ch}_{b,i,s,t}$, $\rho^{ch}_{b,i,s,t}$	Auxiliary binary variable, $\theta^{ch}_{b,i,s,t}, \rho^{ch}_{b,i,s,t} \in \{0,1\}$
$P^{avg}_{j,s}$	Average power demand during demand interval j in station s (kW), $P^{avg}_{j,s} \geq 0$
F^{total}	Total annual system costs ($/year), $F^{total} \geq 0$
$CAPEX$	Total capital costs ($), $CAPEX \geq 0$
$OPEX$	Total daily operational costs ($), $OPEX \geq 0$

(*continued on next page*)

Table 2 (*continued*)

Decision variables	Description
$E^{arr}_{b,i,s}$	Arrival battery energy level of the bus b after trip i in station s (kWh), $E^{arr}_{b,i,s} \geq 0$
$E^{dep}_{b,i,s}$	Departure battery energy level of the bus b before trip i in station s (kWh), $E^{dep}_{b,i,s} \geq 0$
$E^{ESS,l}_{t,s}$	ESS energy level at timeslot t in station s (kWh), $E^{ESS,l}_{t,s} \geq 0$

The types of variables are defined in (30).

$$
\begin{aligned}
&P^{rated,tr}_{s} \in A^{tr}, P^{rated,conv}_{s} \in A^{conv}, P^{rated,st}_{s} \in A^{st}, E^{ESS}_{s} \in A^{ESS}, N^{pil}_{s} \in \mathbb{Z}_{>0}, P^{dem}_{s} \geq 0 \ \forall s \in S \\
&E^{batt}_{b} \in A^{batt} \ \forall b \in B \\
&P^{grid}_{t,}, P^{ESS,ch}_{t,s}, P^{ESS,dis}_{t,s}, P^{st,ch}_{t,s}, P^{conv}_{t,s}, E^{ESS,l}_{t,s} \geq 0 \ \forall s \in S, \forall t \in T \\
&y_{t,s}, z_{t,s} \in \{0,1\} \ \forall s \in S, \forall t \in T \\
&P^{avg}_{j,s} \geq 0 \ \forall s \in S, \forall j \in J \\
&E^{arr}_{b,i,s}, E^{dep}_{b,i,s} \geq 0 \ \forall b \in B, \forall i \in I_b, s \in S \\
&P^{ch}_{b,i,s,t} \geq 0 \ \forall b \in B, i \in I_b, \forall t \in R_{b,i,s}, s \in S \\
&x_{b,i,s,t}, \theta^{ch}_{b,i,s,t}, \rho^{ch}_{b,i,s,t} \in \{0,1\} \quad \forall b \in B, i \in I_b, \forall t \in R_{b,i,s}, s \in S
\end{aligned}
\tag{30}
$$

3.2. Modelling hydrogen fuel cell electric bus system

3.2.1. Problem description

The proposed electrolysis-powered HFCB system configuration model quantifies the optimal hydrogen production, refueling station configuration, and the HFCB fleet that minimizes the total system costs. For the HFCB fleet configuration, the fuel cell size of each bus $\left(E^{BS}_{b}, \forall b \in B\right)$ is estimated. The system involves an on-site hydrogen generation unit to produce, compress, store, and distribute hydrogen for HFCBs. Therefore, the refueling system is only allocated in the depot (i.e., only one hydrogen generation unit to power the fleet), as illustrated in Fig. 3.

The refueling system includes an electricity grid connection through a facility transformer, followed by a power conversion system (PCS) to convert alternative current (AC) to direct current (DC). An electrolyzer utilizes the DC power to break down water (H_2O) into hydrogen (H_2) and oxygen (O_2). The produced hydrogen (H_2) is then compressed by a DC compressor to meet the required pressure for fueling HFCBs and stored in a hydrogen storage (HS) tank. Finally, the stored hydrogen is delivered to HFCBs through dispensers.

The proposed model provides the optimal component sizing of the fueling station at the depot, including the transformer-rated power ($P^{rated,tr}$), the converter rated power ($P^{rated,conv}$), electrolyzer rated power ($P^{rated,elz}$), compressor rated power ($P^{rated,comp}$), hydrogen storage tank capacity (E^{HS}), and the number of fuel dispensers (N^{disp}).

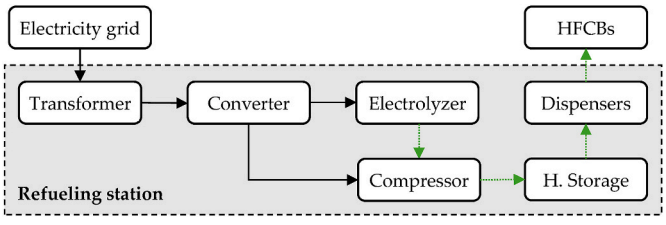

Fig. 3. Schematic diagram of an on-site electrolysis-powered HFCB refueling station (green arrows represent H_2). (For interpretation of the references to colour in this figure legend, the reader is referred to the Web version of this article.)

Generally, the model provides the optimal dispatch for the electrolyzer and compressor and the optimal schedule for fuel production, storage, and utilization stages. Most notably, while hydrogen production occurs throughout the day, hydrogen refueling only takes place overnight at the depot after the fleet has completed all scheduled trips. As such, the proposed model achieves the trade-off between electrolyzer size, storage size, and electricity costs in the optimal system configuration.

Toward this end, a generic HFCB system configuration model is formulated as a mixed integer linear programming model. The notations of the HFCB model are shown in Table 3.

3.2.2. Objective function

The proposed HFCB configuration model aims to minimize the total annual system cost (31), integrally minimizing the CAPEX (32) and OPEX (33).

$$
F^{total} = \frac{r(1+r)^{y}}{(1+r)^{y}-1} CAPEX + N^{days} OPEX \tag{31}
$$

In (32), CAPEX comprises eight costs, including the costs of refueling station construction, transformer, converter, electrolyzer, compressor, HS tank, dispensers, and the HFCBs. Where, $\alpha^{tr}, \alpha^{conv}, \alpha^{elz}$ and α^{comp} are cost factors associated with the component power, α^{HS} is the HS cost factor related to the tank size, α^{disp} is the dispenser cost factor, α^{BS} represents the bus fuel cell storage cost factor, and α^{HFCB} denotes the purchase cost of the HFCB without a tank.

$$
\begin{aligned}
CAPEX = {} & \alpha^{con} + \alpha^{tr} P^{rated,tr} + \alpha^{conv} P^{rated,conv} + \alpha^{elz} P^{rated,elz} + \alpha^{comp} P^{rated,comp} \\
& + \alpha^{HS} E^{HS} + \alpha^{disp} N^{disp} + \sum_{b \in B} \left(\alpha^{BS} E^{BS}_{b} + \alpha^{HFCB} \right)
\end{aligned}
\tag{32}
$$

OPEX is presented in (33) and involves five operational costs. The electricity cost is formulated in the first two terms in (33), similar to the BEB model. The third term denotes the social cost of GHG emissions, while the fourth term presents the electrolyzer operational cost. Where, L^{elz}_{t} is the electrolyzer hydrogen production rate at timeslot t and P^{elz}_{t} is the electrolyzer input power at the timeslot t. The last two terms describe the compressor and HS operational costs, respectively, where

Table 3
HFCB model notations.

Sets	Description
B	Set of Buses, indexed by b
T	Set of day timeslots, indexed by t
R_b	Set of recovery timeslots of bus b overnight
J	Set of daily demand measurement intervals, indexed by j
T_j	Set of timeslots in demand measurement interval j
A^{tr}	Set of potential transformer-rated power values
A^{conv}	Set of potential converter-rated power values
A^{elz}	Set of potential electrolyzer-rated power values
A^{comp}	Set of potential compressor-rated power values
A^{HS}	Set of potential HS tank size values
A^{BS}	Set of potential bus hydrogen tank size values

Parameters	Description	Parameters	Description
r	Discount rate (%)	α^{w}	Water cost ($/kg)
y	Lifespan in years (#)	$\alpha^{elz,op}$	Electrolyzer operational cost ($/kWh)
N^{days}	Number of working days per year (#)	$\alpha^{comp,op}$	Compressor operational cost ($/kWh)
α^{con}	Construction cost ($)	$\alpha^{HS,op}$	HS operational cost ($/kg)
α^{tr}	Transformer cost ($/kW)	ξ^{tr}	Transformer efficiency (%)
α^{conv}	Converter cost ($/kW)	ξ^{conv}	Converter efficiency (%)
α^{comp}	Compressor cost ($/kW)	η^{elz}	Efficiency of the electrolyzer unit (%)
α^{HS}	HS cost ($/kg)	LHV_{H_2}	Lower heat value of hydrogen (kWh/kg)
α^{disp}	Dispenser cost ($/unit)	η^{comp}	Compression efficiency (%)
α^{BS}	Bus HS cost ($/kg)	$\xi^{HS,dis}$	HS dissipation factor (%)
α^{HFCB}	HFCB cost ($/unit)	ξ^{HS}_{min}, ξ^{HS}_{max} ξ^{BS}_{min}, ξ^{BS}_{max}	Limits (%)
α^{elect}_t	Electricity cost during timeslot t ($/kWh)	L^{ref}_{max}	The maximum bus hydrogen refueling rate (kg/hr)
ΔT	Timeslot duration (hr)	l_b	Length of trips of bus b (km)
α^{dem}	Demand charge rate ($/kW)	e^{cons}_b	Hydrogen fuel consumption rate of bus b (kg/km)
α^{em}_t	Grid WTT social cost of GHG emissions during timeslot t ($/kWh)	η^{ref}	Refueling efficiency (%)
$e^{cons,BS}$	Energy consumption rate due to the hydrogen tank	L^{ref}_{min}	The minimum bus hydrogen refueling rate (kg/hr)
α^{elz}	Electrolyzer cost ($/kW)	R	Ideal gas constant (J/mol. K)
T^{elz}	Electrolyzer temperature (K)	k	Polytropic coefficient
$\pi^{H_2}_t$	Electrolyzer hydrogen pressure (bar)	π^{HS}_t	HS pressure (bar)

Decision variables	Description
$P^{rated,tr}$	Transformer rated power (kW), $P^{rated,tr} \in A^{tr}$
$P^{rated,conv}$	Converter rated power (kW), $P^{rated,conv} \in A^{conv}$
$P^{rated,elz}$	Electrolyzer rated power (kW), $P^{rated,elz} \in A^{elz}$
$P^{rated,comp}$	Compressor rated power (kW), $P^{rated,comp} \in A^{comp}$
E^{HS}	HS tank capacity (kg), $E^{HS} \in A^{HS}$
N^{disp}	Number of dispensers (#), $N^{disp} \in Z_{\geq 0}$
E^{BS}_b	Bus fuel cell storage capacity (kg), $E^{BS}_b \in A^{BS}$
P^{grid}_t	Power demand from the grid at timeslot t (kW), $P^{grid}_t \geq 0$
P^{dem}	Peak power demand (kW), $P^{dem} \geq 0$
L^{elz}_t	Electrolyzer hydrogen production rate at timeslot t (kg/hr), $L^{elz}_t \geq 0$
P^{elz}_t	Electrolyzer input power at timeslot t (kW), $P^{elz}_t \geq 0$
P^{comp}_t	Compressor input power at timeslot t (kW), $P^{comp}_t \geq 0$
P^{conv}_t	Converter input power at timeslot t (kW), $P^{conv}_t \geq 0$
L^{dem}_t	Fleet hydrogen demand rate at timeslot t (kg/hr), $L^{dem}_t \geq 0$
$L^{ref}_{b,t}$	Refueling hydrogen rate for bus b during timeslot t (kg/hr), $L^{ref}_{b,t} \geq 0$
$x_{b,t}$	A Binary decision variable indicates whether bus b is refueling during timeslot t or not, $x_{b,t} \in \{0,1\}$
$\theta^{BS}_{b,t}, \rho^{BS}_{b,t}$	Auxiliary binary variable, $\theta^{BS}_{b,t}, \rho^{BS}_{b,t} \in \{0,1\}$

(*continued on next page*)

Table 3 (*continued*)

Decision variables	Description
P_j^{avg}	Average power demand during demand interval j (kW), $P_j^{avg} \geq 0$
F^{total}	Total annual system costs ($/year)
$CAPEX$	Total capital costs ($)
$OPEX$	Total daily operational costs ($)
$\mathrm{MoH_t}$	HS mass of hydrogen (kg)
E_b^{arr}	Arrival mass of hydrogen of the bus b fuel cell storage (kg)
E_b^{dep}	Departure mass of hydrogen of the bus b fuel cell storage (kg)

P_t^{comp} is the compressor input power at the timeslot t.

$$OPEX = \sum_{t\in T}\alpha_t^{elect}\Delta TP_t^{conv} + \alpha^{dem}P^{dem} + \sum_{t\in T}\alpha_t^{em}\Delta TP_t^{conv} + \sum_{t\in T}\left[\alpha^{w}\Delta TL_t^{elz} + \alpha^{elz,op}\Delta TP_t^{elz}\right] + \sum_{t\in T}\alpha^{comp,op}\Delta TP_t^{comp} + \sum_{t\in T}\alpha^{HS,op}\Delta TL_t^{elz} \quad (33)$$

The objective function of the proposed HFCB model in (31) is optimized under a set of constraints presented in (34–57).

3.2.3. HFCB system's constraints

For each HFCB $b \in B$, the mass of hydrogen (MoH) in the bus fuel cell storage follows (34–37). In (34), the MoH in the fuel cell storage of each bus $b \in B$ at the time of departure from the depot (E_b^{dep}) is set to the maximum predefined level. In addition, the arrival MoH on each bus (E_b^{arr}) should be more than a minimum threshold, as presented in (35). For each HFCB, as described in (36), the arrival MoH equals the departure MoH minus the fuel consumption during the scheduled operation, where l_b is the total travelled distance, e_b^{cons} is the fixed energy consumption rate for bus $b \in B$, and $e^{cons,BS}$ denotes the variable energy consumption rate related to the bus fuel cell storage size $\left(E_b^{BS}\right)$. Here, each HFCB is refueling overnight at the depot to reach the maximum level for the next day's operation. Therefore, in (37), the departure MoH equals the summation of the arrival MoH and the refueling amount, where R_b is the recovery timeslots of bus b overnight, η^{ref} is the refueling efficiency, and $L_{b,t}^{ref}$ denotes the refueling hydrogen rate for bus b during timeslot t. Similar to the BEB model in (11–13), the refueling process of the HFCBs should be accomplished in continuous time intervals using Constraints (38-40), where $x_{b,t}$ is a binary decision variable that presents if the HFCB b is refueling in timeslot t or not.

$$E_b^{dep} = \xi_{max}^{BS}E_b^{BS} \quad \forall b \in B \quad (34)$$

$$E_b^{arr} \geq \xi_{min}^{BS}E_b^{BS} \quad \forall b \in B \quad (35)$$

$$E_b^{arr} = E_b^{dep} - l_b\left(e_b^{cons} + e^{cons,BS}E_b^{BS}\right) \quad \forall b \in B \quad (36)$$

$$E_b^{dep} = E_b^{arr} + \sum_{t\in R_b}\eta^{ref}\Delta TL_{b,t}^{ref} \quad \forall b \in B \quad (37)$$

$$\theta_{b,t}^{BS} \geq x_{b,t} - x_{b,t+1} \quad \forall b \in B, \forall t \in R_b \quad (38)$$

$$\rho_{b,t}^{BS} \geq x_{b,t} - x_{b,t-1} \quad \forall b \in B, \forall t \in R_b \quad (39)$$

$$\sum_{t\in R_b}\theta_{b,t}^{BS} = \sum_{t\in R_b}\rho_{b,t}^{BS} \leq 1 \quad \forall b \in B \quad (40)$$

As illustrated in Fig. 3, the power demand from the grid (P_t^{grid}) equals to the power demand of the electrolyzer (P_t^{elz}) and compressor (P_t^{comp}), and the losses of the transformer and converter. This active power balance constraint is emphasized in (41).

$$P_t^{grid} = P_t^{elz} + P_t^{comp} - (1-\xi^{tr})P_{t,s}^{grid} - (1-\xi^{conv})\,P_{t,s}^{conv} \quad \forall t \in T \quad (41)$$

The relation between the power demand from the electricity grid in each timeslot $t \in T$ (P_t^{grid}) and the transformer-rated power is presented in (42). In the same way, (43) denotes the relation between the input power of the converter (P_t^{conv}) and the converter-rated power ($P^{rated,conv}$). Then, in (44), P_t^{conv} should be equal to the product of P_t^{grid} and the transformer efficiency (ξ^{tr}).

$$P_t^{grid} \leq P^{rated,tr} \quad \forall t \in T \quad (42)$$

$$P_t^{conv} \leq P^{rated,conv} \quad \forall t \in T \quad (43)$$

$$P_t^{conv} = \xi^{tr}P_t^{grid} \quad \forall t \in T \quad (44)$$

The electrolyzer's hydrogen production rate at timeslot t (L_t^{elz}) is a function of the electrolyzer's input power at this timeslot t (P_t^{elz}) as described in (45), where η^{elz} is the electrolyzer efficiency and LHV_{H_2} is the lower heat value of hydrogen. Moreover, Equation (46) demonstrates that the operational power of the electrolyzer should be less than its rated power. In (47), the compressor's input power at a given timeslot t (P_t^{comp}) is determined by the hydrogen production rate from the electrolyzer based on the polytrophic model, which serves as the input to the compressor [49]. Additionally, (48) specifies that the compressor's input power must not exceed its rated capacity.

$$L_t^{elz} = \frac{\eta^{elz}}{LHV_{H_2}}\,P_t^{elz} \quad \forall t \in T \quad (45)$$

$$P_t^{elz} \leq P^{rated,elz} \quad \forall t \in T \quad (46)$$

$$P_t^{comp} = \frac{2RT^{elz}kL_t^{elz}}{(k-1)\eta^{comp}}\left[\left(\frac{\pi_t^{HS}}{\sqrt{\pi_t^{H_2}\pi_t^{HS}}}\right)^{\frac{k-1}{k}} - 1\right] \quad \forall t \in T \quad (47)$$

$$P_t^{comp} \leq P^{rated,comp} \quad \forall t \in T \quad (48)$$

The HS tank on the refueling station is constrained by (49-51). The MoH in the HS tank is updated using (49). The MoH in timeslot t ($\mathrm{MoH_t}$) equals the MoH in the previous timeslot $t-1$ ($\mathrm{MoH_{t-1}}$) in addition to the difference between the hydrogen supply from the electrolyzer ($L_t^{elz}\Delta t$) and the hydrogen demand ($L_t^{dem}\Delta t$) to refuel the HFCBs and the dissipation amount ($\xi^{HS,disp}\mathrm{MoH_{t-1}}$). During the operation, $\mathrm{MoH_t}$ must remain within a predefined range associated with the HS tank size, as indicated in (50). Meanwhile, the initial value ($\mathrm{MoH_1}$) is set to the maximum level, as specified in (51).

$$\mathrm{MoH_t} = \mathrm{MoH}_t - 1 + \left(L_t^{elz} - L_t^{dem}\right)\Delta t - \xi^{HS,disp}\mathrm{MoH_{t-1}} \quad \forall t \in T \quad (49)$$

$$\xi_{min}^{HS}E^{HS} \leq \mathrm{MoH_t} \leq \xi_{max}^{HS}E^{HS} \quad \forall t \in T \quad (50)$$

$$\mathrm{MoH_1} = \xi_{max}^{HS}E^{HS} \quad (51)$$

For the refueling station, in (52), the total demand rate at timeslot t (L_t^{dem}) equals the summation of the refueling hydrogen rate for each bus b during timeslot t ($L_{b,t}^{ref}$). In addition, $L_{b,t}^{ref}$ is restricted to a predefined range

using (53) according to the dispenser specification and the compressor pressure. In (54), in the same timeslot t, the number of refueling HFCBs should be less than the number of available dispensers.

$$L_t^{dem} = \sum_{b \in B} L_{b,t}^{ref} \quad \forall t \in T \tag{52}$$

$$L_{min}^{ref} x_{b,t} \leq L_{b,t}^{ref} \leq L_{max}^{ref} x_{b,t} \quad \forall b \in B, t \in R_b \tag{53}$$

$$\sum_{b \in B} x_{b,t} \leq N^{disp} \quad \forall t \in T \tag{54}$$

The peak power demand of the HFCB refueling station is calculated using (55-56).

$$P_j^{avg} = \frac{\sum_{t \in T_j} P_t^{conv}}{|T_j|} \quad \forall j \in J \tag{55}$$

$$P^{dem} \geq P_j^{avg} \quad \forall j \in J \tag{56}$$

The types of variables in the proposed HFCB configuration model are presented in (57).

$$\begin{aligned} &P^{rated,tr} \in A^{tr}, P^{rated,conv} \in A^{conv}, P^{rated,elz} \in A^{elz}, P^{rated,comp} \in A^{comp}, E^{HS} \in A^{HS}, N^{disp} \in Z_{\geq 0}, E_b^{BS} \in A^{BS}, P^{dem} \geq 0 \\ &P_t^{grid}, L_t^{elz}, P_t^{elz}, P_t^{comp}, P_t^{conv}, L_t^{dem} \geq 0 \; \forall t \in T \\ &L_{b,t}^{ref} \geq 0 \; \forall b \in B, \forall t \in R_b \\ &x_{b,t}, \theta_{b,t}^{BS}, \delta_{b,t}^{BS} \in \{0,1\} \; \forall b \in B, \forall t \in R_b \\ &P_j^{avg} \geq 0 \; \forall j \in J \end{aligned} \tag{57}$$

4. Case study

The bus transit network in Belleville City, Ontario, Canada, serves as the case study for the two proposed models. This network has a hub-and-spoke design, with a central station and a depot. The depot is around 2.5 km away from the central station. The transit network includes nine bus routes operated by 11 buses, covering a total of 247 trips each day, starting and ending at the central station. The case study is illustrated in Fig. 4.

The proposed models maintain the number of buses and the current timetable (presented in Table A.1. in Appendix A) to preserve the current service standards. The input parameters for the BEB and HFCB configuration models are presented in Table 4. The electricity chargers (α_t^{elect}) comprises the average energy price and global adjustment per hour, calculated over the course of one year, in Ontario, Canada. The social cost of GHG emissions (α_t^{em}) is estimated using electricity generation data from Ontario, Canada, to assess the WTT GHG emissions and the social cost factor in Canada [63]. This hourly social cost of GHG emissions is calculated based on the average electricity generation mix (e.g., nuclear, natural gas steam reformers, and renewable) in each hour over one year. Notably, the BEB system is solved in two configurations: one with two charging stations (at the terminal and depot), referred to as the BEB opportunity charging model, and one with a single charging station (at the depot), referred to as the BEB overnight charging model. The three models (i.e., BEB opportunity charging, BEB overnight charging, and HFCB overnight charging) are implemented in Python and solved using the GUROBI optimizer on a computer with a 4.9 GHz processor and 32 GB of RAM.

Fig. 4. Considered case study: the bus transit network of Belleville City, Ontario, Canada.

5. Results: systems configuration

The optimal costs of the BEB and HFCB systems are reported in Fig. 5. The total annual system cost of the BEB opportunity charging system is $916,197, which includes 10.3% infrastructure, 71.6% fleet, and 18.1% operation costs. Moreover, the total system cost of the BEB overnight charging system is $1,221,861, with relatively higher fleet cost because of the larger battery capacities. In contrast, the total annual cost of the HFCB overnight refueling system is $2,865,671, including 3.8% infrastructure, 57.0% fleet, and 39.3% operation costs. It is evident that the BEB system is significantly cheaper (at most 43% of the HFCB system cost).

The high cost of the HFCB system is primarily attributed to 1) the cost of HFCB, which is 67% greater than that of the BEB fleet, and 2) operational costs, which are 477.5% higher with respect to the overnight charging case. The operational cost of hydrogen production, compression, and storage is significant compared to the operational cost of BEB chargers. The optimal configurations of the three systems are presented in Table 5 and Fig. 6. Notably, the energy/hydrogen flow in Fig. 6 is for one full day.

For the BEB opportunity charging system design, two charging stations are installed at the depot and the central terminal. The terminal charging station is equipped with a 280-kW transformer, a 260-kW converter, a 350-kWh stationary ESS (ESS's power is the same as the converter) for grid peak demand mitigation, and a high-power charger rated at 1250 kW with six charging outlets. Moreover, the depot has a lower-capacity charging station featuring a 40-kW transformer, a 40-kW converter, and a 40-kW slow charger with one charging pile. Most notably, the depot does not have an ESS deployed. For the BEB overnight charging system, the depot charging station comprises a 400-kW high-power charger, a 400-kW converter, and a 420-kW transformer. This fast charger is used overnight to charge the large batteries that power the fleet throughout the day. Similar to BEB opportunity charging, the ESS loses its cost-saving benefits during overnight charging and is, therefore, not deployed in the depot's overnight charging system.

In comparison, the optimal design of the HFCB overnight refueling

Table 4
BEB Model parameters.

BEB Model parameters			HFCB Model parameters		
Parameters	Value	Reference	Parameters	Value	Reference
r	5.75%	[49]	r	5.75%	[49]
y	15	[64]	y	15	[64]
N^{days}	365	Model specifications	N^{days}	365	Model specification
α^{con}	$75,000	[26]	α^{con}	$75,000	[26]
α^{tr}	500 $/kW	[7]	α^{tr}	500 $/kW	[7]
α^{conv}	120 $/kW	[65]	α^{conv}	120 $/kW	[65]
α^{BC}	300 $/kW	[66]	α^{comp}	7.52 $/kW	[49]
α^{pil}	$13,000	[66]	α^{HS}	124 $/kg	[49]
α^{ESS}	300 $/kWh	[17]	α^{disp}	$152,400	[67]
α^{batt}	500 $/kWh	[68]	α^{BS}	124 $/kg	[49]
α^{BEB}	$550,000	[26]	α^{HFCB}	$1,386,934	[69]
ΔT	5/60	Model Specification	ΔT	5/60	Model Specification
α^{dem}	$0.126	[70]	α^{dem}	$0.126	[70]
μ^{ch}, $\mu^{ESS,ch}$, $\mu^{ESS,dis}$	3	[35]	α^{w}	0.08 $/kg	[49]
$P^{max.pil}$	500 kW	Model Specification	$\alpha^{elz.op}$	0.072 $/kWh	Model Specification
ξ^{tr}	95%	[21,36]	$\alpha^{comp.op}$	0.1128 $/kWh	[49]
ξ^{conv}	95%	Model Specification	$\alpha^{HS.op}$	2.48 $/kg	[49]
ξ^{ESS}_{min}, ξ^{ESS}_{max}, ξ^{batt}_{min}, ξ^{batt}_{max}	20%, 90%	[71]	α^{elz}	784 $/kW	[49]
η^{ch}, $\eta^{ESS,dis}$, $\eta^{ESS,ch}$	95%	[21,36]	ξ^{tr}	95%	[21,36]
$P^{max.ESS}$	2500 kW	Model Specification	ξ^{conv}	95%	Model Specification
$P^{ch.min}$	10 kW	Model Specification	L^{ref}_{min}	10	Model Specification
A^{tr}	{10, 20, …, 2500}	Model Specification	η^{elz}	60%	[72]
A^{conv}	{10, 20, …, 2500}	Model Specification	LHV_{H_2}	33.33 kWh/kg	[72]
A^{st}	{10, 20, …, 2500}	Model Specification	η^{comp}	63%	[49]
A^{ESS}	{50, 100, …, 2500}	Model Specification	$\xi^{HS.disp}$	0.0006%	[49]
A^{batt}	{50, 100, …, 700}	Model Specification	R	8.31 J/mol.K	[49]
			T^{elz}	323 K	[49]
			k	1.4	[49]
			ξ^{HS}_{min}	10%	[72]
			ξ^{HS}_{max}	100%	[72]
			L^{ref}_{max}	180	Model Specification
			ξ^{BS}_{min}	10%	Model Specification
			ξ^{BS}_{max}	100%	Model Specification
			η^{ref}	0.995	Model Specification
			A^{tr}	{10, 20, …, 2500}	Model Specification
			A^{conv}	{10, 20, …, 2500}	Model Specification
			A^{elz}	{10, 20, …, 2500}	Model Specification
			A^{comp}	{10, 20, …, 2500}	Model Specification
			A^{HS}	{10, 20, …, 2500}	Model Specification
			A^{BS}	{30, 35, …, 70}	Model Specification

Please note that $1 = 1.3 CAD and 1 £ = $1.27.

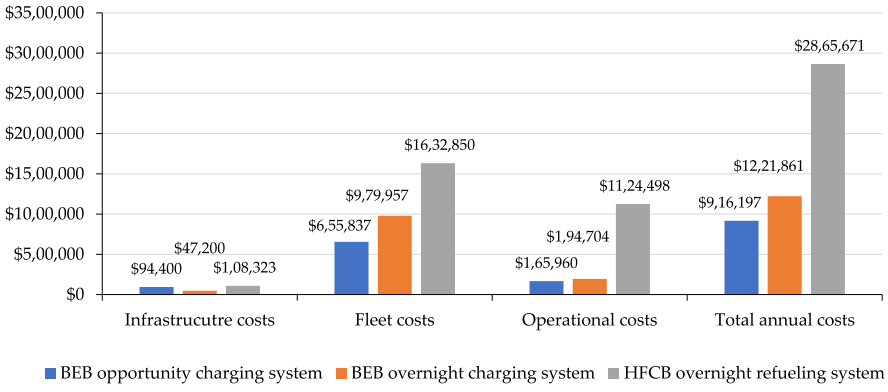

Fig. 5. Cost comparison between BEB and HFCB systems.

station consists of a relatively higher-rated power transformer (650 kW), converter (620 kW), and electrolyzer (550 kW), which are necessary for the hydrogen production required to satisfy the HFCB fleet operation. A 40-kW compressor is used to increase the hydrogen pressure and store it in a 90 kg HS tank.

For fleet configuration, the BEB opportunity charging system and the HFCB overnight refueling system tend to reduce the battery/fuel-cell-tank sizes to mitigate the fleet costs. The BEB opportunity system utilizes small batteries (i.e., 50 kWh and 100 kWh) and extends the operational range through en-route charging at the central terminal during

Table 5
Comparison between BEB and HFCB systems components.

Parameters		BEB opportunity charging system	BEB overnight charging system	HFCB overnight refueling system
Costs	CAPEX ($)	$ 750,237	$ 1,027,157	$ 1,741,173
	OPEX ($)	$ 165,960	$ 194,704	$ 1,124,498
	Total annual costs ($)	$ 916,197	$ 1,221,861	$ 2,865,671
Infrastructure configuration	Transformer power (kW)	1 × 280 (Terminal) 1 × 40 (depot)	1 × 420	650
	Converter power (kW)	1 × 260 (Terminal) 1 × 40 (depot)	1 × 400	620
	Electrolyzer power (kW)	NA	NA	550
	Compressor power (kW)	NA	NA	40
	Charger power (kW)	1 × 1250 (Terminal) 1 × 40 (depot)	1 × 400	NA
	ESS/HS capacity	350 kWh (Terminal)	0	90 kg
	Number of outlets/disposals (#)	6 (Terminal) 1 (depot)	1	1
Fleet configuration		5 × 50 kWh 6 × 100 kWh	1 × 200 kWh & 1 × 300 kWh 1 × 450 kWh & 1 × 500 kWh 1 × 550 kWh & 1 × 600 kWh 1 × 700 kWh & 1 × 800 kWh 1 × 900 kWh & 1 × 1100 kWh 1 × 1150 kWh	8 × 30 kg 1 × 35 kg 2 × 40 kg
Annual GHG emissions (tCo_2e)		119.04	114.93	362.89

the recovery time between scheduled trips. For HFCB buses, a 30 kg fuel tank is used on eight HFCBs out of 11, as this mass of hydrogen is sufficient to satisfy the operational range of these buses. However, the BEB overnight charging system requires large batteries to satisfy the operational timetable.

Table 5 shows that the annual WTT GHG emissions of the HFCB system (362.89 tCO_2e) are around three times higher than those of the BEB system with the highest emissions (119.04 tCO_2e). This is attributed to the power required for hydrogen production and the associated emissions. In this respect, using electricity to charge batteries directly is considered greener than electricity grid-based hydrogen, considering the average GHG intensity in Ontario's electricity profile (30 gCO_2e/kWh in 2023).

From an operation perspective, the proposed model provides a detailed optimal charging/refueling schedule, power demand distribution, and power/hydrogen consumption at every timeslot. For the BEB opportunity charging system, the daily energy demand is illustrated in Fig. 7, with a total of 4345 kWh. The energy demand for depot overnight charging is only 574 kWh, with an hourly peak power demand of 38 kW. However, the energy demand for the terminal is relatively higher at 3771 kWh, which is utilized for opportunity charging. The ESS at the terminal helps reduce the peak power demand from the electricity grid to 258.9 kW, even with 1250 kW charger-rated power. The daily ESS energy level is presented in Appendix B, highlighting the charging and discharging periods. It shows that the ESS mainly charges overnight at a low electricity rate and is utilized during BEB operation to reduce peak power demand. More details on the daily grid power demand from the charging stations are presented in Appendix C. For the BEB overnight charging system, the energy demand is 5450 kWh, which is 25% more than the opportunity system. Moreover, the peak power demand of the charging station reaches 386.6 kW. This is attributed to the rise in energy consumption rate resulting from increased battery capacity, which also increases battery mass.

In contrast, the HFCB system has a relatively higher energy demand, as described in Fig. 7, with 613.7 kW hourly peak power demand. The HFCB system's power demand is distributed between the electrolyzer and compressor. For the electrolyzer, the power demand is almost steady at 550 kW with a hydrogen production rate of 9.9 kg/h. The compressor demands 33 kW to compress the hydrogen in a 90 kg HS tank. For more details about the operational schedules, the MoH in the HS tank is presented in Appendix D, and the station's refueling rate is shown in Appendix E.

6. Systems competitiveness: HFCB or BEB

A sensitivity analysis of the HFCB system is conducted to assess how changes in the HFCB fleet and operational cost parameters influence the total annual system costs and to identify the cost ranges that allow the HFCB system to compete financially with the BEB system. Notably, since the optimal design for the BEB system is opportunity charging, aligning with real-world practices that favor opportunity charging for BEBs and depot charging for HFCBs, the comparison here will focus on the BEB opportunity charging system versus the HFCB overnight charging system.

Fleet and operational costs are selected in this sensitivity analysis as they are the main contributors to the total annual system costs of the HFCB system. For each parameter, 20 scenarios are analyzed, including the baseline (i.e., 400 total scenarios for all parameters). These scenarios are generated by applying multipliers from 0.1 to 2.0, in 0.1 increments, with 1.0 representing the base model.

Fig. 8 shows that the HFCB system is economically competitive with the BEB system cost under three scenarios, as follows:

1) Reducing the HFCB unit cost to 10% combined with an operational cost reduction between 10% and 50% of the current values. In this case, the HFCB cost is set to $138,693, and the operational cost should be reduced by at least 50%.
2) Reducing the HFCB unit cost to 20% of the current cost with an operational cost reduction to 10%, 20%, or 30% of the current value. In this case, the HFCB cost is set to $277,387, with at least a 70% reduction in the operational costs.
3) The HFCB cost is 30% of the used value, and the operational cost is reduced to 10%. In this case, the HFCB cost only needs to be reduced to $416,080. However, the operational costs must be decreased by at least 90%.

Overall, these thresholds indicate that reducing the operational costs for H_2 production is fundamental to promoting the economic viability of the HFCB transit systems along with the HFCB unit cost.

For more details, the results of all scenarios are illustrated in Appendix F. One of the main approaches to reducing the HFCB unit cost is through incentive and rebate programs to accelerate the adoption of zero-emission vehicles. However, these incentives should be tailored to the specific technology. In other words, HFCB incentives should be based on the cost difference between HFCBs and diesel buses rather than

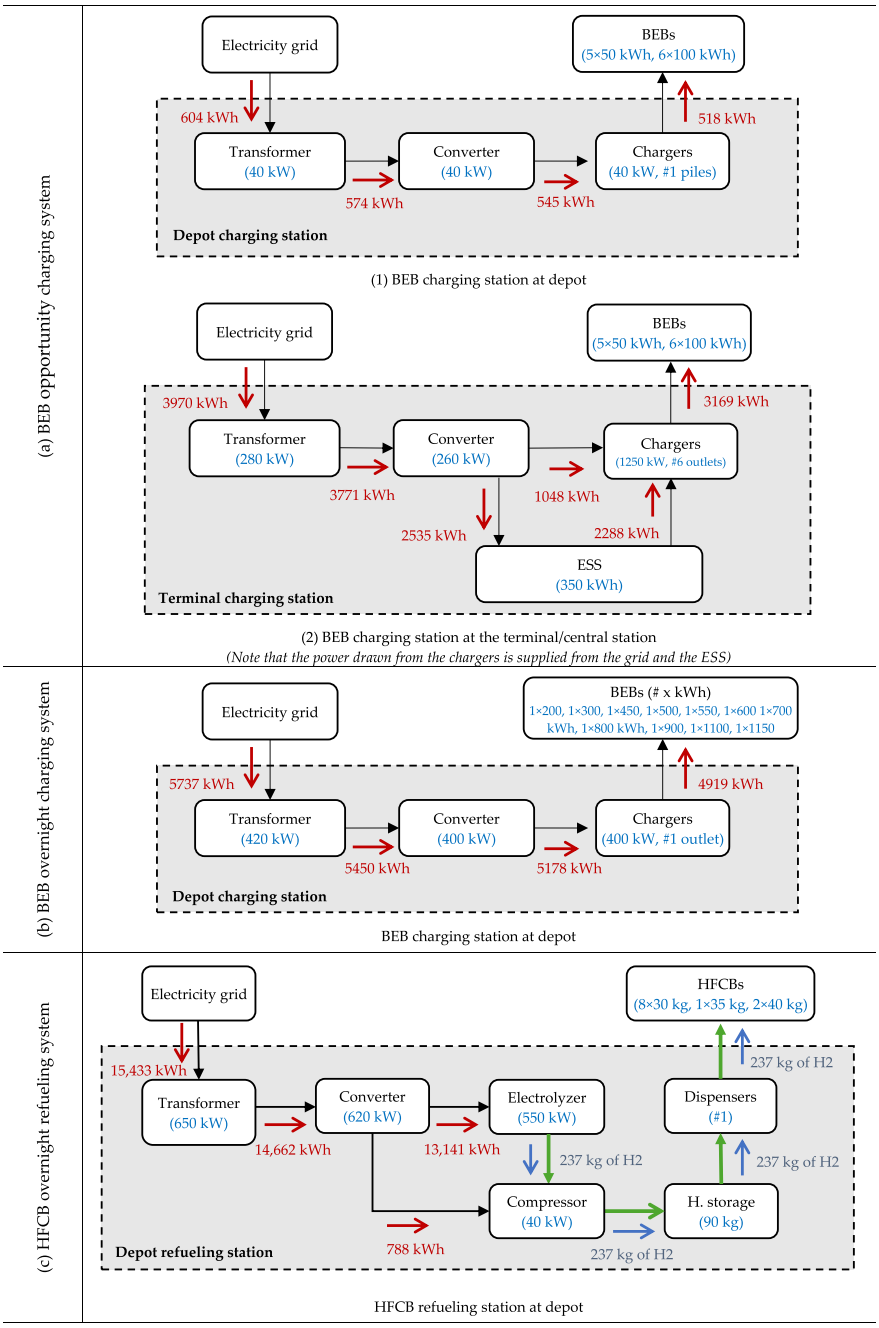

Fig. 6. Refueling/charging station configuration with daily energy flows (a) BEB opportunity charging system, (b) BEB overnight charging system, and (c) HFCB overnight refueling system.

being equal to those for BEBs. This is a viable solution until HFCB technology is well-established. Additionally, research efforts should be extensively focused on advancing HFCB technology to reduce its cost and make it comparable with other technologies. For operational costs, subsidizing electricity costs is a viable solution, such as through carbon offset rebates, along with research focused on increasing hydrogen production efficiency (e.g., electrolyzers).

Compared to existing literature, our findings are aligned with relevant studies comparing the two systems. From a system cost perspective, the HFCB system cost is reported to be 48% [5], 25% [59], and 55% [60] more expensive than BEB systems. Our findings indicate the HFCB system is 135% more expensive than the BEB overnight charging system. This higher percentage in our results is due to the inclusion of fleet costs and configuration in our comparison, which are not accounted for in previous studies. From a cost perspective, the work in Ref. [59] recommended that reducing electricity prices and electrolyzer capital costs could lead to a 50% reduction in HFCB system costs, thereby enhancing its economic competitiveness. We also recommend, based on the sensitivity analysis, that a significant reduction in the HFCB unit and electricity costs is required to economically compete with BEB systems. Notably, our study assumes equal lifespans for the fuel cell and batteries, and the salvage value of the components, such as the fuel cell and batteries, is excluded from the calculations.

7. Conclusion

This study contributes to advancing the research on planning and configuring zero-emission electric buses in public transportation. The

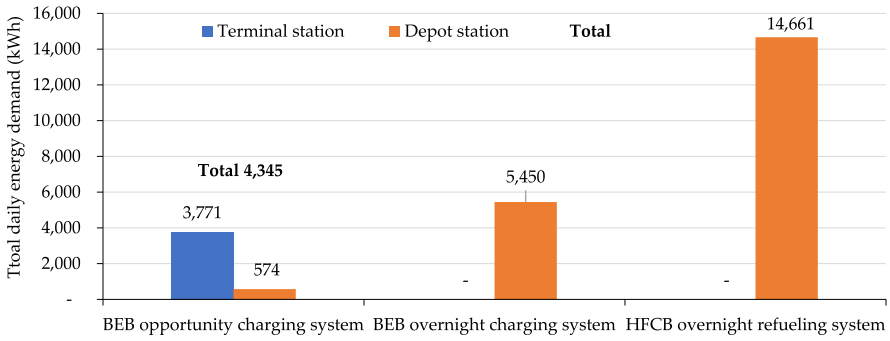

Fig. 7. Total daily energy demand of the three systems.

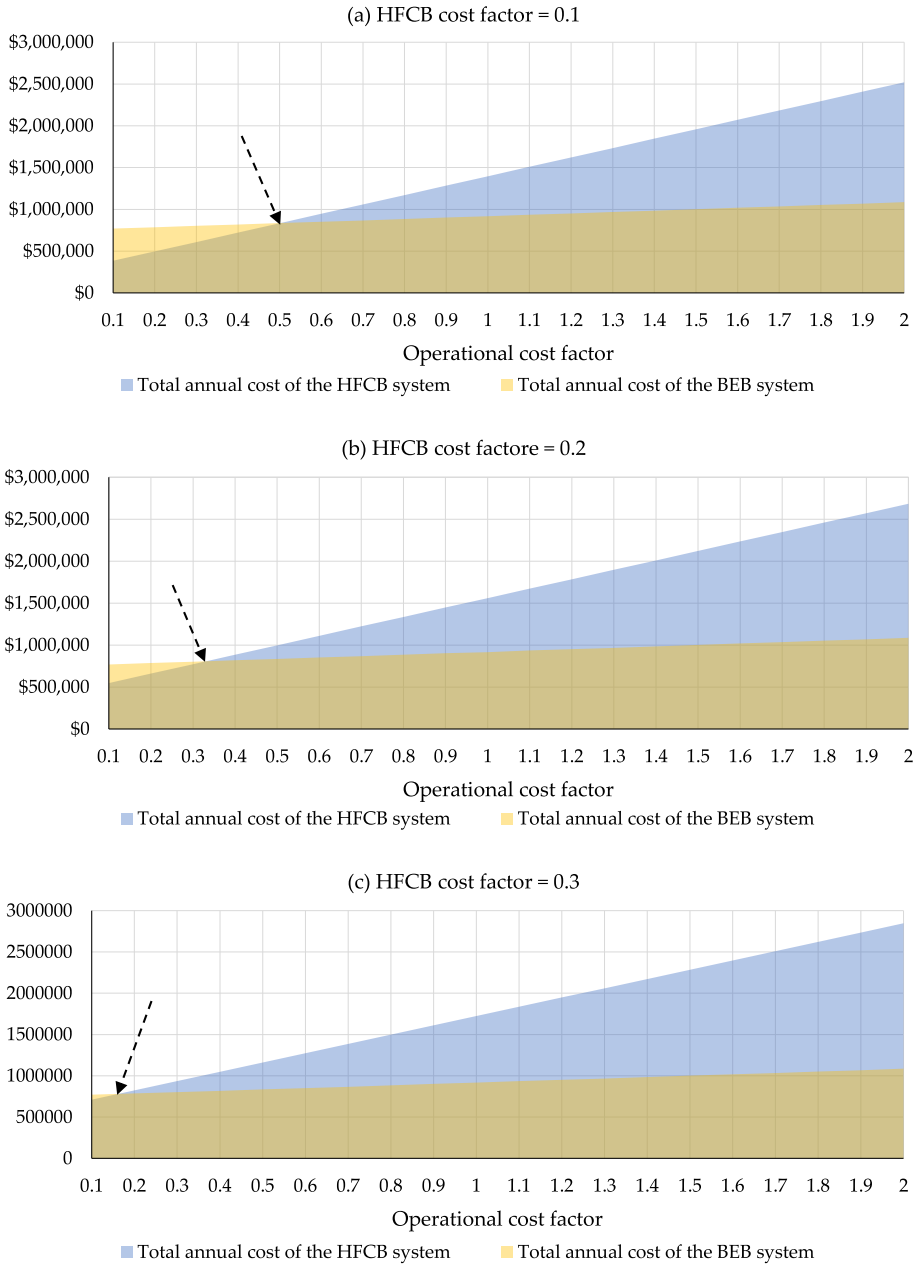

Fig. 8. The total annual system cost under various operational costs with specific HFCB cost factor (a) 0.1 (b) 0.2 (C) 0.3.

configurations of two dominant technologies (BEB and HFCB) are optimized using mixed-integer linear programming models. Each model minimizes the total annual system costs, including CAPEX (i.e., charging/refueling station and fleet) and OPEX (i.e., electricity costs and social cost of GHG emissions). Moreover, the proposed models not only optimize the system configuration but also optimize the energy/fuel management systems without jeopardizing the existing timetables. These models are tested using data from real-world case study, offering valuable insights and recommendations.

The findings indicate that each technology has a different configuration, energy management systems, GHG emissions footprint, and total system costs. Comparatively, the opportunity BEB system is the most cost-effective and has the lowest impact on the electrical grid. The total annual system costs of the BEB opportunity charging system are 25% and 68% less than the BEB overnight charging system and HFCB overnight refueling system, respectively. Moreover, the energy demand and the peak power demand of the BEB opportunity charging system are less than the other two systems. However, from an environmental perspective, the GHG emissions of the BEB overnight charging system are 3% and 68% less than the BEB opportunity charging system and HFCB overnight refueling system, respectively. Therefore, within the Belleville city network, the BEB system offers more significant economic and environmental advantages than the HFCB system.

Across all systems, fleet costs are the highest, followed by operational and infrastructure costs. A sensitivity analysis is conducted to test the economic competitiveness of the HFCB system. The rationale is to examine how variations in hydrogen bus unit cost and operational costs impact the system costs. Moreover, the sensitivity analysis highlights thresholds at which the HFCB system can achieve competitiveness with the BEB system. The findings show that a substantial reduction in the HFCB unit cost (at least 70%) coupled with a decrease in operational costs (at least 50%) are necessary for the HFCB system to become economically competitive with BEB systems.

Overall, the developed models offer multiple contributions to advancing transit network electrification and comparing the system configuration of two transit electrification technologies. These models will assist stakeholders in making informed decisions about transit network electrification, including the choice of the appropriate technology, necessary infrastructure, operations, and associated capital and operational costs. From an energy perspective, the study also contributes to the optimization of energy management and configuration for both on-site hydrogen production and energy storage systems.

Nevertheless, we recognize that there is room for further refinements. First, integrating renewable energy sources (RESs), such as photovoltaic panels, into the BEB and HFCB systems can significantly reduce GHG emissions and the impact on the electricity grid. Second, grid-connected on-site hydrogen production is not the sole method of supplying the HFCB refueling station. Developing a flexible model that accommodates other hydrogen sourcing methods (off-grid "islanded" on-site hydrogen production and transported supply) will comprehensively compare these options and the BEB system. Thirdly, accounting for traffic congestion and its impact on energy consumption, as well as the fleet mix, introduces complexities that are worth investigating. Finally, the differences in degradation and lifespan of batteries and fuel cells can impact the total cost of ownership comparison between the two systems. These points will be explored in our future work.

CRediT authorship contribution statement

Ahmed Foda: Writing – review & editing, Writing – original draft, Visualization, Validation, Software, Methodology, Investigation, Formal analysis, Conceptualization. **Moataz Mohamed:** Writing – review & editing, Writing – original draft, Visualization, Validation, Supervision, Resources, Project administration, Methodology, Investigation, Funding acquisition, Conceptualization. **Hany E.Z. Farag:** Writing – review & editing, Validation, Methodology, Investigation, Conceptualization. **Patrick Jochem:** Writing – review & editing, Validation, Investigation, Conceptualization. **Elkafi Hassini:** Writing – review & editing, Supervision, Funding acquisition.

Declaration of competing interest

The authors declare that they have no known competing financial interests or personal relationships that could have appeared to influence the work reported in this paper.

Acknowledgment

This work was supported by the Natural Sciences and Engineering Research Council of Canada (NSERC) [Grant No: RGPIN-2018-05994] and NSERC Alliance grant.

Appendix A. Supplementary data

Supplementary data to this article can be found online at https://doi.org/10.1016/j.ijhydene.2025.02.251.

References

[1] ECCC. Environment and Climate Change Canada. Greenhouse gas emissions. https://www.canada.ca/en/environment-climate-change/services/environmental-indicators/greenhouse-gas-emissions.html; 2022. 2024.
[2] Isik M, Dodder R, Kaplan PO. Transportation emissions scenarios for New York City under different carbon intensities of electricity and electric vehicle adoption rates. Nat Energy 2021;6:92–104.
[3] Mahmoud M, Garnett R, Ferguson M, Kanaroglou P. Electric buses: a review of alternative powertrains. Renew Sustain Energy Rev 2016;62:673–84.
[4] Foda A. Battery electric bus transit planning: operations research, applied mathematical modelling, and advanced optimization techniques. McMaster University; 2024.
[5] Peng Z, Wang Z, Wang S, Chen A, Zhuge C. Fuel and infrastructure options for electrifying public transit: a data-driven micro-simulation approach. Appl Energy 2024;369.
[6] Fortune. Electric bus market. https://www.fortunebusinessinsights.com/electric-bus-market-102021; 2024. 2024.
[7] Foda A, Abdelaty H, Mohamed M, El-Saadany E. A generic cost-utility-emission optimization for electric bus transit infrastructure planning and charging scheduling. Energy 2023;277.
[8] Foda A, Mohamed M. The impacts of optimization approaches on BEB system configuration in transit. Transp Policy 2024;151:12–23.
[9] Lee H, Kim A, Lee A, Lee B, Lim H. Optimized H2 fueling station arrangement model based on total cost of ownership (TCO) of fuel cell electric vehicle (FCEV). Int J Hydrogen Energy 2021;46:34116–27.
[10] Greene DL, Ogden JM, Lin Z. Challenges in the designing, planning and deployment of hydrogen refueling infrastructure for fuel cell electric vehicles. eTransportation 2020;6.
[11] Gim J, Kim M, Ahn C. Energy management control strategy for saving trip costs of fuel cell/battery electric vehicles. Energies 2022;15.
[12] Ji J, Bie Y, Wang L. Optimal electric bus fleet scheduling for a route with charging facility sharing. Transport Res C Emerg Technol 2023:147.
[13] Zhang M, Yang M. Optimal electric bus scheduling considering battery degradation effect and charging facility capacity. Transport Lett 2024:1–11.
[14] Liu X, Liu X, Zhang X, Zhou Y, Chen J, Ma X. Optimal location planning of electric bus charging stations with integrated photovoltaic and energy storage system. Comput-Aided Civ Inf 2022;38:1424–46.
[15] Liu Z, Song Z, He Y. Planning of fast-charging stations for a battery electric bus system under energy consumption uncertainty. Transp Res Rec 2018;2672:96–107.
[16] Gairola P, Nezamuddin N. Optimization framework for integrated battery electric bus planning and charging scheduling, vol. 118. Transport Res D-Tr E; 2023.
[17] He Y, Song Z, Liu Z. Fast-charging station deployment for battery electric bus systems considering electricity demand charges. Sustain Cities Soc 2019;48.
[18] Lotfi M, Pereira P, Paterakis N, Gabbar HA, Catalao JPS. Optimizing charging infrastructures of electric bus routes to minimize total ownership cost. In: 2020 20th ieee international conference on environment and electrical engineering and 2020 4th ieee industrial and commercial power systems europe (eeeic/I&cps europe); 2020.
[19] Kharouf M, Abdelaziz M. Battery electric bus system schedule-based optimization. Ieee Electr Pow Ener 2021:402–7.
[20] Zhou Y, Meng Q, Ong GP, Wang H. Electric bus charging scheduling on a bus network. Transport Res C Emerg Technol 2024:161.
[21] Liu K, Gao H, Liang Z, Zhao M, Li C. Optimal charging strategy for large-scale electric buses considering resource constraints, vol. 99. Transport Res D-Tr E; 2021.
[22] Hanna MO, Shaaban MF, Salama MMA. Comprehensive transition plan for battery-electric bus fleets considering utility constraints. IEEE Trans Ind Appl 2023:1–12.

[23] Lin Y, Zhang K, Shen Z-JM, Ye B, Miao L. Multistage large-scale charging station planning for electric buses considering transportation network and power grid. Transport Res C Emerg Technol 2019;107:423–43.
[24] Wang Y, Liao F, Bi J, Lu C. Optimal battery electric bus system planning considering heterogeneous vehicles, opportunity charging, and battery degradation. Renew Energy 2024;237.
[25] Shehabeldeen A, Foda A, Mohamed M. A multi-stage optimization of battery electric bus transit with battery degradation. Energy 2024;299.
[26] Foda A, Mohamed M, Farag H, El-Saadany E. A resilient battery electric bus transit system configuration. Nat Commun 2023;14:8279.
[27] Abdelaty H, Foda A, Mohamed M. The robustness of battery electric bus transit networks under charging infrastructure disruptions. Sustain-Basel 2023;15.
[28] Zhou Y, Wang H, Wang Y, Li R. Robust optimization for integrated planning of electric-bus charger deployment and charging scheduling, vol. 110. Transport Res D-Tr E; 2022.
[29] Wang YS, Huang YX, Xu JP, Barclay N. Optimal recharging scheduling for urban electric buses: a case study in Davis, vol. 100. Transport Res E-Log; 2017. p. 115–32.
[30] Wu X, Feng Q, Bai C, Lai CS, Jia Y, Lai LL. A novel fast-charging stations locational planning model for electric bus transit system. Energy 2021;224.
[31] El-Taweel NA, Mohamed M, Farag HE. Optimal design of charging stations for electrified transit networks. Ieee Transp Elect C. 2017:786–91.
[32] Zhong L, Zeng Z, Huang Z, Shi X, Bie Y. Joint optimization of electric bus charging and energy storage system scheduling. Front Eng Manag 2024;11:676–96.
[33] Liu X, Yeh S, Plötz P, Ma W, Li F, Ma X. Electric bus charging scheduling problem considering charging infrastructure integrated with solar photovoltaic and energy storage systems. Transport Res E Logist Transport Rev 2024:187.
[34] Luke J, Ribeiro MGdC, Martin S, Balogun E, Cezar GV, Pavone M, et al. Optimal coordination of electric buses and battery storage for achieving a 24/7 carbon-free electrified fleet. Appl Energy 2025;377.
[35] Liu K, Gao H, Wang Y, Feng T, Li C. Robust charging strategies for electric bus fleets under energy consumption uncertainty, vol. 104. Transport Res D-Tr E; 2022.
[36] Zaneti LAL, Arias NB, de Almeida MC, Rider MJ. Sustainable charging schedule of electric buses in a University Campus: a rolling horizon approach. Renew Sustain Energy Rev 2022;161.
[37] Foda A, Mohamed M, Bakr M. Dynamic surrogate trip-level energy model for electric bus transit system optimization. Transp Res Rec 2022;2677:513–28.
[38] Jahic A, Eskander M, Schulz D. Charging schedule for load peak minimization on large-scale electric bus depots. Appl Sci-Basel 2019;9.
[39] Rupp M, Rieke C, Handschuh N, Kuperjans I. Economic and ecological optimization of electric bus charging considering variable electricity prices and CO2eq intensities, vol. 81. Transport Res D-Tr E; 2020.
[40] He Y, Liu Z, Song Z. Integrated charging infrastructure planning and charging scheduling for battery electric bus systems, vol. 111. Transport Res D-Tr E; 2022.
[41] Campíñez-Romero S, Colmenar-Santos A, Pérez-Molina C, Mur-Pérez F. A hydrogen refuelling stations infrastructure deployment for cities supported on fuel cell taxi roll-out. Energy 2018;148:1018–31.
[42] Geçici E, Güler MG, Bilgiç T. Multi-period planning of hydrogen refuelling stations using flow data: a case study for Istanbul. Int J Hydrogen Energy 2022;47:40138–55.
[43] Tafakkori K, Bozorgi-Amiri A, Yousefi-Babadi A. Sustainable generalized refueling station location problem under uncertainty. Sustain Cities Soc 2020;63.
[44] Zhao Q, Kelley SB, Xiao F, Kuby MJ. A multi-scale framework for fuel station location: from highways to street intersections, vol. 74. Transport Res D-Tr E; 2019. p. 48–64.
[45] Lin R-H, Ye Z-Z, Wu B-D. A review of hydrogen station location models. Int J Hydrogen Energy 2020;45:20176–83.
[46] Kuvvetli Y. Multi-objective and multi-period hydrogen refueling station location problem. Int J Hydrogen Energy 2020;45:30845–58.
[47] Li S, Long J, Sui PC, Hou Z, Chahine R, Xiao J. Addition of hydrogen refueling for fuel cell bus fleet to existing natural gas stations: a case study in Wuhan, China. Int J Energy Res 2019;43:7557–72.
[48] El-Hamalawy AF, Farag HEZ, Asif A. Optimal design of grid-connected green hydrogen plants considering electrolysis internal parameters and battery energy storage systems. Energy Convers Manag 2024;302.
[49] Abomazid AM, El-Taweel NA, Farag HEZ. Optimal energy management of hydrogen energy facility using integrated battery energy storage and solar photovoltaic systems. IEEE Trans Sustain Energy 2022;13:1457–68.
[50] Grüger F, Dylewski L, Robinius M, Stolten D. Carsharing with fuel cell vehicles: sizing hydrogen refueling stations based on refueling behavior. Appl Energy 2018;228:1540–9.
[51] Li J, Lin J, Song Y, Xing X, Fu C. Operation optimization of power to hydrogen and heat (P2HH) in ADN coordinated with the district heating network. IEEE Trans Sustain Energy 2019;10:1672–83.
[52] Sriyakul T, Jermsittiparsert K. Risk-constrained design of autonomous hybrid refueling station for hydrogen and electric vehicles using information gap decision theory. Int J Hydrogen Energy 2021;46:1682–93.
[53] Coppitters D, Verleysen K, De Paepe W, Contino F. How can renewable hydrogen compete with diesel in public transport? Robust design optimization of a hydrogen refueling station under techno-economic and environmental uncertainty. Appl Energy 2022;312.
[54] Gunawan TA, Williamson I, Raine D, Monaghan RFD. Decarbonising city bus networks in Ireland with renewable hydrogen. Int J Hydrogen Energy 2021;46:28870–86.
[55] Syré AM, Shyposha P, Freisem L, Pollak A, Göhlich D. Comparative life cycle assessment of battery and fuel cell electric cars, trucks, and buses. World Electr Vehicle J 2024;15.
[56] Ahmadi P, Raeesi M, Changizian S, Teimouri A, Khoshnevisan A. Lifecycle assessment of diesel, diesel-electric and hydrogen fuel cell transit buses with fuel cell degradation and battery aging using machine learning techniques. Energy 2022;259.
[57] Hensher DA, Wei E, Balbontin C. Comparative assessment of zero emission electric and hydrogen buses in Australia, vol. 102. Transport Res D-Tr E; 2022.
[58] Borghetti F, Longo M, Bonera M, Libretti M, Somaschini C, Martinelli V, et al. Battery electric buses or fuel cell electric buses? A decarbonization case study in the city of brescia, Italy. Infrastructures 2023;8.
[59] Caponi R, Bocci E, Del Zotto L. On-site hydrogen refuelling station techno-economic model for a fleet of fuel cell buses. Int J Hydrogen Energy 2024;71:691–700.
[60] Rozzi E, Giglio E, Moscoloni C, Novo R, Mattiazzo G, Lanzini A. Comparative study of electric and hydrogen mobility infrastructures for sustainable public transport: a PyPSA optimization for a remote island context. Int J Hydrogen Energy 2024;80:516–27.
[61] Abdelshafy AM, Samir O, Elnozahy A, Ali AFM. Innovative energy management strategy of battery and fuel cell buses charging station. Energy Convers Manag 2024;315.
[62] El-Taweel NA, Farag HEZ, Mohamed M. Integrated utility-transit model for optimal configuration of battery electric bus systems. IEEE Syst J 2020;14:738–48.
[63] ECCC. Environment and Climate Change Canada. Social cost of greenhouse gas emissions. https://www.canada.ca/en/environment-climate-change/services/climate-change/science-research-data/social-cost-ghg.html; 2023. 2024.
[64] Coban HH. Smart steps towards sustainable transportation: profitability of electric road system. Balkan J Electr Comput Eng 2023;11:88–99.
[65] El-Taweel NA, Khani H, Farag HEZ. Optimal sizing and scheduling of LOHC-based generation and storage plants for concurrent services to transportation sector and ancillary services market. IEEE Trans Sustain Energy 2020;11:1381–93.
[66] Liu Z, Song Z, He Y. Economic analysis of on-route fast charging for battery electric buses: case study in Utah. Transp Res Rec 2019;2673:119–30.
[67] Pure Energy Centre. Hydrogen fuelling station. https://pureenergycentre.com/hydrogen-products-pure-energy-centre/hydrogen-fuelling-station/; 2024. 2024.
[68] Quarles N, Kockelman KM, Mohamed M. Costs and benefits of electrifying and automating bus transit fleets. Sustain-Basel 2020;12.
[69] CUTRIC. Brampton transit ZEB implementation strategy and rollout plan: net zero by 2041. 2024.
[70] Kadri A, Mohammadi F. Demand charges minimization for Ontario class-A customers based on the optimization of energy storage system. 2020 ieee Canadian conference on electrical and computer engineering (ccece). 2020. p. 1–4.
[71] He Y, Liu ZC, Song ZQ. Optimal charging scheduling and management for a fast-charging battery electric bus system, vol. 142. Transport Res E-Log; 2020.
[72] Al-obaidi AA, Farag HEZ, El-Saadany EF. Estimation-based online adaptive management of distribution feeder congestion using electrolysis hydrogen refueling stations. IEEE Trans Ind Inf 2024;20:7459–70.